7-2015

Computational prediction of remodeling of collagen fiber network in articular cartilage under dynamic unconfined compression

Juan Andres Coello Amado
University of Texas-Pan American

COMPUTATIONAL PREDICTION OF REMODELING OF COLLAGEN FIBER NETWORK IN ARTICULAR CARTILAGE UNDER DYNAMIC UNCONFINED COMPRESSION

A Thesis

by

JUAN ANDRES COELLO AMADO

Submitted to the Graduate School of
The University of Texas-Pan American
In partial fulfillment of the requirements for the degree of

MASTER OF SCIENCE

July 2015

Major Subject: Mechanical Engineering

COMPUTATIONAL PREDICTION OF REMODELING OF COLLAGEN FIBER NETWORK IN ARTICULAR CARTILAGE UNDER DYNAMIC UNCONFINED COMPRESSION

A Thesis
by
JUAN ANDRES COELLO AMADO

COMMITTEE MEMBERS

Dr. Reza Shirazi
Committee Chair

Dr. Dumitru Caruntu
Committee Member

Dr. Arturo Fuentes
Committee Member

Dr. Horacio Vasquez
Committee Member

July 2015

ABSTRACT

Coello Amado, Juan Andres, Computational Prediction of Remodeling of Collagen Fiber Network in Articular Cartilage under Dynamic Unconfined Compression. Master of Science (MS), July 2015, 63 pp, 4 tables, 30 figures, 45 references, 43 titles.

A poroelastic finite element model of a heterogeneous cartilage disk was created based on previous studies and experimental setups; this allows us to study cartilage behavior under dynamic unconfined compression. Previous studies have used a Post Hoc approach, which consist of searching for patterns or relationships between predicted mechanical parameters obtained through computational and experimental results. Our goal in this study is to take the same Post-Hoc approach and identify patterns between predicted mechanical parameters, such as fiber strain or stress, and experimentally-measured collagen fiber distribution (i.e. reorientation of fibers under dynamic unconfined compression). After computational predictions were obtained, it was observed that stress and pore pressure, in addition to fiber strain, are key to triggering the reorientation of collagen fibers in the cartilage tissue.

ACKNOWLEDGMENTS

I would like to give my sincerest expression of gratitude to my mentor and advisor Dr. Reza Shirazi as without his encouragement, guidance and understanding throughout this year and a half of work, I would not have been able to finish this project. Without him, I would not have been able to address the project clearly, and to be able to fully understand the behavior of articular cartilage. Also, I thank him for his patience while I was trying to learn the new software ABAQUS to be able to perform all this work, which finally paid off.

I would also like to thank Kevin Yamauchi for without his help in understanding his work and feedback regarding our project, we would not have been able to move on, and also thank you for providing the different data and files we needed for our computational models. Also, thanks to Dr. Stephen Klisch for helping guide our project in the correct direction and providing feedback as we were analyzing our results.

Finally, I would like to thank my beautiful wife for without her support and understanding through long work days on campus and long hours at night at home I would have gone crazy through this whole project, as she kept me sane as she is. Also, I want to thank my parents for supporting me throughout my studies and always encouraging me to achieve greatness, I know it must have been difficult for you supporting me from there.

TABLE OF CONTENTS

Page

ABSTRACT…… iii

ACKNOWLEDGEMENTS…… iv

TABLE OF CONTENTS…… v

LIST OF TABLES…….. viii

LIST OF FIGURES……..... ix

CHAPTER I. INTRODUCTION…… 1

CHAPTER II. BACKGROUND REVIEW…… 5

2.1 Remodeling in articular cartilage…….. 6

2.1.1 Collagen remodeling…… 7

2.2 Quantitative polarized light microscopy……..... 7

2.3 Biphasic theory…… 8

CHAPTER III. EXPERIMENTAL SETUP……..... 9

3.1 Harvesting and culture……..... 9

3.2 Biochemical analysis……. 11

3.3 Quantitative polarized light microscopy information……..... 13

CHAPTER IV. COMPUTATIONAL APPROACH…….. 15

4.1 Kinematics…… 15

4.2 Biphasic theory……. 17

4.3 Constitutive stresses…….. 19

4.3.1 Glycosaminoglycan (GAG) stress and Jacobian matrix……..... 21

4.3.2 Collagen fiber network stress and Jacobian matrix……..... 22

4.3.2.1 Collagen fiber distribution function……. 24

4.3.3 Ground substance matrix (MAT) stress and Jacobian matrix……..... 28

4.3.4 Immobility constraint……..... 29

4.4 Collagen remodeling – post hoc approach……..... 29

4.5 Computational implementation……. 30

4.6 Geometry, mesh creation and boundary conditions…….. 31

4.7 Material properties…… 33

4.8 Spherical discretization using pyramids……..... 35

4.9 Simulation steps…… 35

4.9.1 Free swelling step……..... 36

4.9.2 Ramp step…… 36

4.9.3 Sinusoidal step……. 37

4.10 Solver……..... 38

4.11 Post processing……..... 38

4.12 Computational requirements……..... 40

CHAPTER V. RESULTS……..... 41

5.1 Interpolation of experimental results…..…….. 41

5.2 Finite element analysis predictions……..... 43

5.3 Correlations between experiment and theory…….…….…….…..... 49

CHAPTER VI. DISCUSSION……..... 53

REFERENCES……..... 56

BIOGRAPHICAL SKETCH…….. 63

LIST OF TABLES

Page

Table 3.1: Experimental group classification. D0 is the untreated control group, FSB is the free-swelling in IGF-1 medium group and S10+D are the group treated with dynamic confined compression. 10

Table 4.1: Experimental data for GAG and collagen density for day 0 and day 6. A linear interpolation was used to determine GAG and collagen density for days 2 through 5..... 34

Table 4.2: Material properties required for the computational models. The angle (α) and standard deviation provided are for day 0.. 34

Table 4.3: Average collagen fiber angles for day 6, for the different regions of interest (ROI). This data, alongside the initial fiber angle data from table 4.3, was used to interpolate and obtain the collagen fiber angles for days 2 through 5..... 35

LIST OF FIGURES

Page

Figure 3.1: The inner region and outer region were analyzed separately to study their composition 11

Figure 3.2: The results were separated into 6 regions of interest, where ROI 1 is located at the inner region at r = 0 and the following ROI's are moving outward in the radial direction until the periphery is reached. 14

Figure 4.1: Particle motion of a body B, the two vectors denoted by X and x, track the position of a particle X from the reference to the current configuration. 15

Figure 4.2: The solid matrix must reach a stress free equilibrium condition from the stress free reference configuration of the different constituent elements, for where each will undergo an initial deformation 21

Figure 4.3: Representation of a unit sphere which is used to model collagen fibers in cartilage; this will be defined at each material point to establish a distribution of collagen fibers. 23

Figure 4.4: Observing the unit sphere in 2-D we have the unit circle, because we are accounting for angle theta only due to symmetry. 25

Figure 4.5: Geometry, boundary conditions loading steps and material properties must be given to ABAQUS to be able to obtain prediction of results. UMAT is used to assign complex material properties. 31

Figure 4.6: Tissue growth representation to justify the use of symmetry to reduce the cartilage disk model to a quarter-disk. Dashed lined represents the deformed cartilage disk.. 32
Figure 4.7: Computational representation of a quarter-disk with the 960 assigned elements 33
Figure 4.8: ABAQUS will determine the necessary deformation needed for COL and MAT to be able to balance the swelling stress of GAG; this will provide a stress free configuration. The height h_0 is defined experimentally by the samples geometry. The equilibrium height h_e is needed to obtain the displacements/strains used for the subsequent steps. 36
Figure 4.9: A continuous 10% compression is applied to the cartilage disk; the magnitude of the strain is calculated from the new height h_e of the model. 37
Figure 4.10: A sinusoidal displacement is applied parting from the static offset of the 10% compressive strain applied in the previous step, this magnitude of the displacement is calculated from the new height h_e. 38
Figure 4.11: The results obtained from the predicted outputs are from the elements located in the Center (inner region) and the Edge (outer region) of the quarter-disk, because of the heterogeneity of the model 39
Figure 4.12: The dynamic loading is applied for 5 cycles of 10 seconds each because after this cycle it reaches steady state; the last cycle is used to study the predicted output obtained. 39
Figure 5.1: Experimental results of collagen volume fraction in the inner region of the cartilage disk. For our studies 90° was establish as being parallel to the articular surface..... 42
Figure 5.2: Experimental results of collagen volume fraction in the outer region of the cartilage disk. For our studies 90° was establish as being parallel to the articular surface..... 42

Figure 5.3: Computational prediction of maximum fiber strain in the inner region, obtained for each pyramidal element of the unit sphere. We see an increase in strain throughout the 6 days of culture.. 45
Figure 5.4: Computational prediction of maximum fiber strain in the outer region, obtained for each pyramidal element of the unit sphere. We see an increase in strain throughout the 6 days of culture.. 45
Figure 5.5: Computational prediction of pore pressure in the inner region of the cartilage disk, for the 5th cycle of dynamic loading for 6 days.. 46
Figure 5.6: Computational prediction of pore pressure in the outer region of the cartilage disk, for the 5th cycle of dynamic loading for 6 days.. 46
Figure 5.7: Normal stress in the radial direction in the inner region. Results obtained from computational predictions of AC models, for the 5th cycle of the dynamic loading step for each day of culture. 47
Figure 5.8: Normal stress in the radial direction outer region. Results obtained from computational predictions of AC models, for the 5th cycle of the dynamic loading step for each day of culture. 47
Figure 5.9: Fluid velocity magnitude experienced within the cartilage tissue in the inner region, accounted for the 5th cycle of the dynamic loading step for the 6 days... 48
Figure 5.10: Fluid velocity magnitude experienced within the cartilage tissue in the outer region, accounted for the 5th cycle of the dynamic loading step for the 6 days.. 48
Figure 5.11: Changes in measured volume fraction and predicted pore pressure in the inner region of cartilage during six days of culture.. 50

Figure 5.12: Changes in measured volume fraction and predicted pore pressure in the outer region of cartilage during six days of culture.. 50
Figure 5.13: Changes in measured volume fraction and predicted radial stress in the inner region of cartilage during six days of culture.. 51
Figure 5.14: Changes in measured volume fraction and predicted radial stress in the outer region of cartilage during six days of culture.. 51
Figure 5.15: Changes in measured volume fraction and predicted fiber strain in the inner region of cartilage during six days of culture. 52
Figure 5.16: Changes in measured volume fraction and predicted fiber strain in the outer region of cartilage during six days of culture. 52

CHAPTER I

INTRODUCTION

Articular cartilage (AC) is a layer low friction soft tissue, with load bearing capabilities which lies at the end of bones in synovial joints. AC allows for pain free movement as it provides wear resistance and shock absorption for decades [1, 3]. AC varies in a lot of aspects (properties, thickness, etc.) within the same joint, among different joints and among species; however, in all synovial joints it has the same components, structure and functions. Even though AC provides substantial advantages for joints, it has a very limited ability to repair itself due to his avascular nature (lack of red blood cells) and low metabolic activity. Injuries and degenerative conditions can compromise these functions resulting in pain and disabilities which are characterized by osteoarthritis and can lead to loss or degradation of cartilage [1, 2, 3]. Arthritis is the most common cause of disability. In 2003, arthritis in the US resulted in an estimated 128 billion in medical care costs and lost earnings, and 52.5 million (22.7%) of adults ages greater than 18 self-reported doctor diagnosed arthritis. By the year 2030 nearly 67 million adults are projected to have self-reported, doctor diagnosed arthritis and in addition 25 million will have arthritis attributed activity limitations [4-6].

Tissue engineering in cartilage is and has been an active area of study to bring biologically active tissue substitutes into clinical use; they offer the potential to provide benefits beyond those of the current repair procedures [7]. All current surgical interventions do not give

the best efficacy and once degeneration has progressed to a progressive osteoarthritis the only available solution is a total knee replacement [8]. In vitro cartilage tissue engineering can work on creating a more durable and functional replacement of a damaged or degraded AC tissue that can be more likely to survive the mechanical conditions in a joint after implementation. The idea is to develop a replacement that has a structure and composition resembling native cartilage and yielding similar mechanical behavior.

Stresses and strain in AC must be determined to understand the complexity in the tissue and one of the most common methods to do this is by the use of the Finite Element Analysis (FEA). Models can range from simple ones to complex models that account for all individual components or constituents, given that if one constituent is removed it alters the remaining constituents [10]. One should always try and use the simplest models that will be sufficient to obtain the data needed (i.e. having a homogeneous model rather than a heterogeneous model if there is not a lot of variation in results). Using Finite Element Analysis to do calculations can be a powerful tool to study cartilage mechanical behavior, understand cartilage functions, and develop methods for treatments and repairs [9]. Even though experimental procedures are needed to give information to the computational models using AC FEA Models can help prevent the continued use of experimental procedures and samples and man hours that cost a lot of money and thus reducing some experimental cost and focusing on results obtained from such models.

The composition of articular cartilage is complex [11], the biomechanical properties of the tissues are anisotropic (i.e. properties dependent on directions), heterogeneous (i.e. properties are dependent on locations), asymmetric (i.e. there is tension and compression asymmetry) and nonlinear (i.e. geometric nonlinearity because of large deformations and material nonlinearity because of a nonlinear stress strain relation) [14]. AC is composed primarily of

Glycosaminoglycan (GAG) and Collagen, the former are primarily responsible of resisting compressive loads and the latter are responsible for resisting tensile and shear loads.
Growth and remodeling are two processes that transform the cartilage from an immature state to a mature state, in vivo (i.e. within the human body). Interstitial tissue growth must account for both, growth and remodeling, because the accumulation of a single component will change the overall tissue structure and mechanical properties. Tissue growth is basically defined as the increase in tissue size due to the accumulation of one or more solid tissue components similar to the ones already present [12].

Tissue growth can be accomplished using growth factors, which are biologically active polypeptides that are produced by the body and can stimulate cellular division, growth and differentiation. Therefore growth factors can offer promising treatments for enhanced regeneration of cartilage in situations of widespread cartilage loss as it occurs in osteoarthritis [13, 45].

One of the most used and most common growth factor is the Insulin-like Growth Factor-I (IGF-I), this type of factor induces a lot of anabolic effects and decreases catabolic responses. IGF-I has the ability to simulate matrix synthesis with the inability to decrease matrix catabolism. In animals test, this growth factor has led to enhanced repair of extensive cartilage defects [13, 45]. Tissue remodeling can be defined as a change in tissue composition and or structure of tissue components. Tissue remodeling is the change in tissue composition or structure of its tissue components (i.e. reorientation of collagen fibers or increase in GAG density). There are many factors that can affect remodeling within the tissue, some of which can mechanical stimuli applied to cartilage tissue i.e. dynamic confined or unconfined compression, shear and tensile tests [14, 15], but also some mechanical parameters of the tissue have been

identified to be triggers or that can be correlated with tissue remodeling such as relative interstitial fluid velocity and maximum principle strain.

Previous studies have used a Post Hoc approach, which consist of searching for patterns or relationships between predicted mechanical parameters and experimental results.

Our goal in the present study is to take the same Post Hoc approach and identify the relationships between mechanical parameters that may affect remodeling of collagen fiber network under dynamic unconfined compression. The hypothesis of the present study is that maximum fiber strain triggers the remodeling of collagen fiber network in articular cartilage. The objectives of the current study are hence set to (a) develop different finite element models of cartilage for 6 days of culture, (b) study these models to identify patterns and relationships between predicted mechanical parameters and previously-measured collagen distribution, (c) suggest variable(s) triggering collagen remodeling.

CHAPTER II

BACKGROUND REVIEW

Articular cartilage (AC) is considered as a solid matrix saturated with interstitial fluid (water). This solid matrix consists of chondrocytes which are embedded in an extracellular matrix (ECM). This ECM is composed of collagen molecules and negatively charged proteoglycans (PG). The mechanical properties of articular cartilage are mainly dependent on this ECM. [9]. The PG is composed of glycosaminoglycan's (GAG) a central protein with negative fixed charge density attached covalently as side chains (i.e. they form a bottlebrush configuration to form PG), because of this fixed charged density the concentration of cations inside the tissue will be higher than the surrounding (it will attract and retain water within the AC tissue) which will cause swelling of the tissue, and normally known as a osmotic pressure [16], this swelling of the tissue will pre-stress the collagen network and thus resist the compressive loads [17]. Collagen (COL) will normally account for most of the dry weight in AC, and the strength of the tissue will depend a lot on the cross linkage of collagen that will form network of fibers.

Four zones that can be visible by a light microscope in articular cartilage, the superficial zone, the transitional zone, the radial zone and the calcified zone; collagen fibrils have been seen to form a random network but some preferred patterns as seen from Transmission Electron

Microscope (TEM) have been assessed through previous works, for example, in the superficial zone the fibers have a tendency to be parallel to the articular surface, they have been seen to be in perpendicular in the radial or deep zone and in the middle zone and have been observed to be isotropically distributed [18].

2.1 Remodeling in articular cartilage

In chapter 1 it was explained what tissue remodeling entailed and a Post-Hoc approach that can be used to determine triggers to remodeling within the cartilage tissue. GAG and collagen are the most predominant components of the solid matrix in articular cartilage therefore there is the importance to understand their behavior under different conditions as this can be key to a successful engineered cartilage.

Previous experimental studies observed that GAG density increases from the inner region to the outer region of the cartilage disk [10]. Buschmann et al. [29] performed computational studies to understand this remodeling of GAG in AC. The predicted results were studied using a Post-Hoc approach as they compared experimental results of GAG with computational predictions from the models and determined that interstitial fluid velocity is the parameter that triggers GAG remodeling past a certain threshold; a distinctive pattern was observed in the studies between experimental results of GAG and computational predictions of fluid velocity where regions that showed an experimental GAG density increase also experienced an increase or a high interstitial fluid velocity [29].

Previous studies performed by Kevin Yamauchi [10] used information from Buschmann et al. [29] studies and derived AC remodeling laws that are applied computationally which related interstitial fluid velocity with GAG density; his studies resulted in a close approximate

match between computational predictions of GAG density and experimental results having fluid velocity as the parameter that triggers the remodeling of GAG in articular cartilage under dynamic unconfined compression. These results can be found in [10].

2.1.1 Collagen remodeling

Collagen fibers tend to orient to some preferred direction depending on the zone they are located at, i.e. parallel to the articular surface in the superficial zone, and perpendicular to the subchondral bone in the deep zone; this reorientation of collagen fibers can be seen as evolving, as the cartilage is maturing, from the superficial to the deep zone [18]. There are many parameters that can be correlated with the re-orientation of collagen fibers, some of which can be maximum fiber strain and Cauchy strain [10, 19, 20]. Studies have used finite element models along with derived remodeling laws to determine if maximum fiber strain is the mechanical parameter that triggers collagen remodeling. Such predictions were not able to match experimentally-measured collagen distribution with computational predictions of collagen distribution. This, however, does not mean that maximum fiber strain is not the mechanical parameter that triggers the reorientation of collagen fibrils in AC [10].

2.2 Quantitative polarized light microscopy

Quantitative polarized light microscopy is a type of microscopy that has been used to experimentally assess the orientation collagen fibers. In qPLM, the state of polarization of a light beam is generally modified when it is reflected or transmitted through a material, this change will carry information about the structure of the material. This is normally used to provide information about specimen birefringence in fields as diverse as materials science,

crystallographic and biology. Cartilage is a birefringent material due to the cylindrical shape of the collagen fibers therefore the samples can be imaged using qPLM; the resulting signal can be analyzed to assess for the orientation of the fibers [21].

2.3 Biphasic theory

Articular Cartilage is considered a biphasic material, as it shows a solid phase (formed by glycosaminoglycan's (GAG), collagen (COL) and a other components of the solid matrix which are group in one parameter called the ground substance matrix, the latter serves as the component the accounts for anything that is not GAG or collagen in the solid matrix of the tissue) and a fluid phase (normally the interstitial fluid surrounding the solid phase); given this, the biphasic theory is a theory that will consider that an intrinsic incompressible solid is saturated with an incompressible inviscid fluid, it has been successfully used to study articular cartilage mechanical responses [22]. This first major biphasic model is given by Mow et al. in 1980 [23]. A small review of the early biphasic models for articular cartilage can be found in [23]. Studies have concluded that under physiological loadings AC will be in a nonlinear stress strain range, therefore large strains are seen [24] and because of these large strains, finite deformation biphasic theories were developed [25,26]. In this study the models used are based upon these finite deformation biphasic theories but adding a continuous distribution of collagen fiber [27].

To be able to implement biphasic theories, study the behavior of cartilage and the remodeling of collagen experimental information is needed in order to perform FE analysis.

CHAPTER III

EXPERIMENTAL SETUP

Experimental data is needed in order to provide input parameters to our finite element models of articular cartilage and be able to test our hypothesis; we will need a set of parameters such as GAG and collagen density, collagen fiber distributions and other material properties. The experimental data and measurements were obtained from our colleagues in procedures explained in [10, 27, 28] and will be briefly summarize here.

3.1 Harvesting and culture

Blocks of articular cartilage were obtained and harvested of patellofemoral groove of fresh bovine knees from newborn calves (approx. 1-3 week old). Cores of 2.5 mm were extracted from the blocks and cut to 1 mm thick disk maintaining the articular surface was intact.

Every sample taken was allowed to free-swell in a phosphate buffered saline. After the free swelling stage, geometric measurements were taken under sterile conditions to be able to assess the disk thickness (using a laser micrometer), wet weight (using an electronic balance) and diameter. After these geometric measurements were recorded the samples were divided into different experimental groups, the ones that had the most uniform thickness were taken into a dynamically loaded group where compressive loadings are to be applied to the samples, and this classification can be seen in Table 3.1 below.

Table 3.1: Experimental group classification. D0 is the untreated control group, FSB is the free-swelling in IGF-1 medium group and S10+D are the group treated with dynamic confined compression.

#	Name	Growth Factor	Treatment	Duration	Days of Culture
0	D0	-	-	-	-
1	FSB	IGF-1	FS	24 hours - on	6
2	S10 + D	IGF-1	S10 + D	8 hours - on 16 hours - off	6

Kevin Yamauchi designed a custom bioreactor as part of his objectives during his master thesis in [10]; this bioreactor was designed to be able to apply a dynamic unconfined compression to the samples during the culture stage.

The dynamically loaded samples had a continuous loading which had a 10% compressive strain as a static offset and directly afterwards a sinusoidal displacement with a ± 2% strain (amplitude) and a frequency of 0.1 Hz performed for 8 hours per day of culture for 6 days of culture, the remaining 16 hours of the day the sample was allowed to free swell each day of culture. The selection of parameters for the experimental application of dynamic loading has been validated through previous studies of using a range of parameters, some of which can be found in [14, 29, 30] and therefore our colleagues used the same conditions, mentioned here, for amplitude and frequency [10, 27- 29] having these set of parameters as the most appropriate ones for the sinusoidal loading. The growth factor used for these experiments was IGF-1 with a concentration of 50ng/ml and cultured in a medium with specifications found in [10]. After the 6 days of culture, geometric measurements were once again taken and recorded.

3.2 Biochemical analysis

Using a dermal punch a 1.5mm diameter section was removed from the samples, this was performed to detect radial difference, and so, the inner and outer portion of the samples were studied individually. To obtain the GAG mass techniques that consisted on using Dimethylmethilne blue with procedures detailed in [31] was used; collagen mass was determined using Hydroxyprolone using methods described in [32].

The densities for COL and GAG were reported as mass normalized initial and final wet weight. Collagen total volume fraction was calculated assuming that the true density of collagen is 1.436 g/cm^3 as determined in [33].

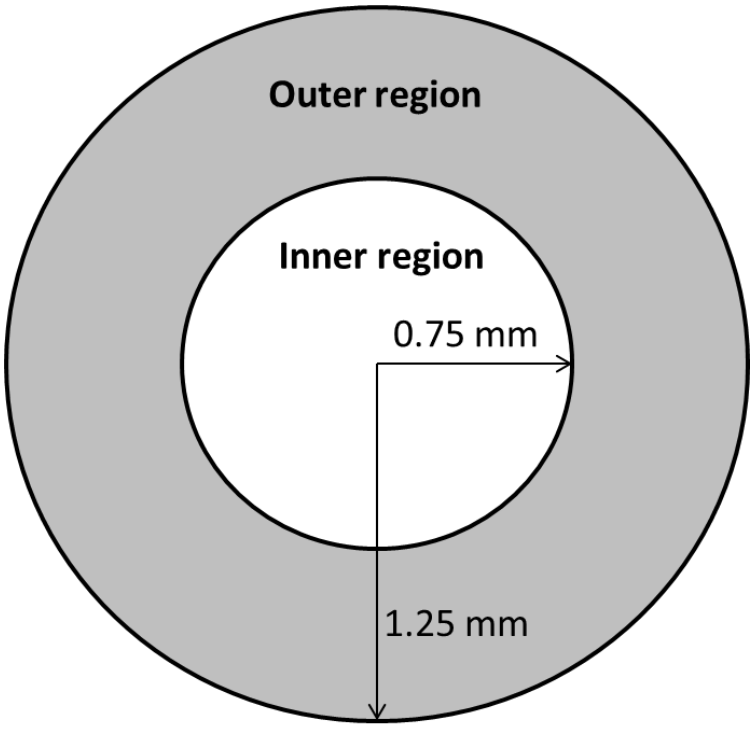

Figure 3.1: The inner region and outer region were analyzed separately to study their composition.

To determine GAG density based upon measured density presented as mass normalized wet weight of GAG Kevin Yamauchi derived the following relationship in [34].

The concentration of GAG is reported as mass normalized wet weight as mentioned

$$\rho_{ww}^{PG} = 100 \times \left(\frac{m_{GAG}}{m_{total}}\right) \tag{3.1}$$

The apparent density is defined as density is defined

$$\rho = 100 \times \left(\frac{m_{GAG}}{m_{total}}\right) \tag{3.2}$$

So, the apparent GAG density will be in units of cg/mL

$$\rho^{PG} = \frac{m_{GAG}}{m_{sample}} \tag{3.3}$$

Substituting equation (3.1) in equation (3.3) it can be derived that

$$\rho^{PG} = \frac{\frac{\rho_{ww}^{PG}}{100} \times m_{sample}}{m_{sample}/\rho_{cartilage}} \tag{3.4}$$

It's assumed that the density of cartilage will be the same as the density of water which is

$$\rho_{cartilage} = \rho_{water} = 1\ g/mL \tag{3.5}$$

Por density of GAG will now be

$$\rho^{PG} = \frac{\rho_{ww}^{PG}}{100} \times 1\frac{g}{mL} \tag{3.6}$$

Converting to proper units

$$\rho^{PG} = \frac{\rho_{ww}^{PG}}{100} \times 1\frac{g}{mL} \times \left[\frac{100cg}{1g}\right] \tag{3.7}$$

And so

$$\rho^{PG} = \rho_{ww}^{PG} \times 1\frac{cg}{mL} \tag{3.8}$$

The experimentally reported GAG density per wet weight can be used to defined the aparent GAG density which will be needed as a material property .

In the same manner, the volume fraction of collagen needs to be determined to be able to obtain the distirbution of collagen fibers [34].

Volume fraction can be defined as the volume of the constituent divided by the total volume of all the constituents

$$\emptyset = \frac{V_{constituent}}{V_{total}} \tag{3.9}$$

In terms of collagen

$$\emptyset^{COL} = \frac{V_{COL}}{V_{total}} \tag{3.10}$$

And applying the equation for density to obtain volume this can be written again as

$$\emptyset^{COL} = \frac{m_{COL}/\rho_{COL}}{m_{sample}/\rho_{cartilage}} \tag{3.11}$$

As mentioned before, the contents are reported as normalized wet weight, so

$$\rho_{ww}^{COL} = 100 \times \left(\frac{m_{COL}}{m_{sample}}\right) \rightarrow m_{COL} = \frac{\rho_{ww}^{COL} \times m_{sample}}{100} \tag{3.12}$$

If we substitute equation (3.12) into equation (3.11) we get

$$\emptyset^{COL} = \frac{\left(\frac{\rho_{ww}^{COL} \times m_{sample}}{100}\right)/\rho_{COL}}{m_{sample}/\rho_{cartilage}} \tag{3.13}$$

Simplifying will give us

$$\emptyset^{COL} = \frac{(\rho_{ww}^{COL})}{100} \times \frac{\rho_{cartilage}}{\rho_{COL}} \tag{3.14}$$

Using the true density of cartilage to be 1.436 g/mL as in [57] and the density of cartilage assumed to be the same as the density of water as in equation (3.5) the collagen volume fraction can be obtained in terms of the experimentally obtained density of collagen per wet weight.

$$\emptyset^{COL} = 0.006964 \times \rho_{ww}^{COL} \tag{3.15}$$

3.3 Quantitative polarized light microscopy information

The way the average angles for collagen fibers was assed is as follows. From the dynamic unconfined compression samples four were taken to be imaged using qPLM, these samples were cut in half in the sagittal plane (i.e. a vertical plane that divides the body into a right and left

half). The samples were imaged using four fields of view, the images obtained were the post processed to obtain the average fiber angles of each pixel in the image, and they were grouped into regions of interest (ROI) that considered the full thickness and a width of approx. 200 microns. Afterwards a mean standard deviation was calculated for each ROI. These regions of interest refer to areas of the inner and outer region of the cartilage; ROI 1 & 2 refer to the inner region and ROI 5 & 6 refer to the outer region and so we have experimental information of collagen fibers from inner to outer region of the cartilage samples.

The experimental information obtained through different methods described in this chapter is used for the computational FE models of articular cartilage that will be presented in chapter 4

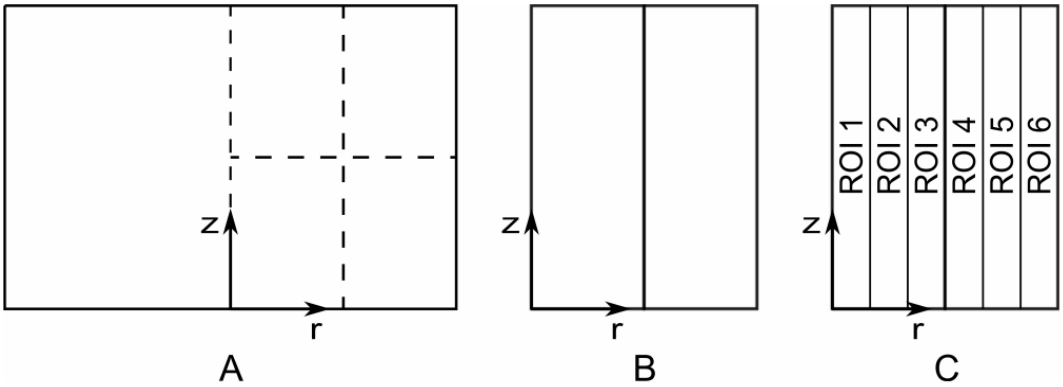

Figure 3.2: The results were separated into 6 regions of interest, where ROI 1 is located at the inner region at r = 0 and the following ROI's are moving outward in the radial direction until the periphery is reached.

CHAPTER IV

COMPUTATIONAL APPROACH

4.1 Kinematics

Consider a continuous body B of a specific and known geometry which will occupy a reference configuration (undeformed configuration) κ_0 (B), such body B will have geometric changes that are known as a deformation, since B is a continuous body it will mean that the loads applied to it are time dependent, the region that is occupied by the continuum at a given time t is called a configuration and denoted by κ, therefore it's called a reference configuration, at different instants of time the body B will occupy different configurations. At some time *t*, B will occupy a new region known as the current configuration (deformed configuration) κ (B) [35].

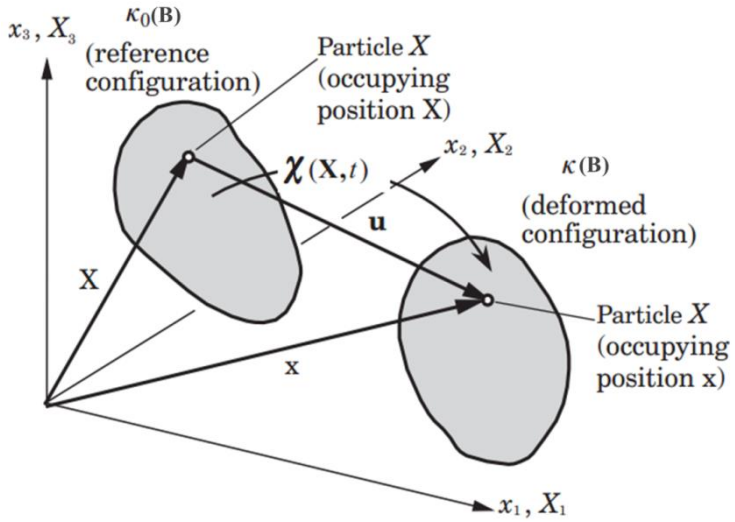

Figure 4.1: Particle motion of a body B, the two vectors denoted by X and x, track the position of a particle X from the reference to the current configuration.

The material point called Particle ***X*** is located at a position **X** denoted by its vector **X** in the reference configuration $\kappa_0(B)$. The same particle ***X*** is located at a position x denoted by its vector x in the current configuration $\kappa(B)$. The mapping of the Body B going from $\kappa_0(B)$ to $\kappa(B)$ is called deformation mapping, thus the motion of the material points on B can be described by

$$\mathbf{x} = \chi(\mathbf{X},t) \tag{4.16}$$

The displacement vector pf the particle *X* on the same moment of the Body B going from the Reference Configuration $\kappa_0(B)$ to the current configuration $\kappa(B)$ is given by

$$u = x - X \tag{4.17}$$

The deformation gradient tensor F is

$$\mathbf{F} = \frac{\partial \mathbf{x}}{\partial \mathbf{X}} \tag{4.18}$$

The right Cauchy-Green deformation tensor C is part of the finite strain theory and is related to the deformation gradient tensor F

$$\mathbf{C} = \mathbf{F}^{\mathbf{T}}\mathbf{F} \tag{4.19}$$

The Lagrangian strain tensor E is related to the right Cauchy-Green deformation tensor by the following relation

$$\mathbf{E} = \frac{1}{2}(\mathbf{C} - \mathbf{I}) \tag{4.20}$$

Where I is the well know Identity tensor

The determinant of the deformation gradient tensor **F** is called the Jacobian of motion and can be seen as the change in volume of body B from the reference (undeformed) configuration to the current (deformed) configuration and is given by

$$J = det(\mathbf{F}) \tag{4.21}$$

Here $det(\cdot)$ is the determinant operator

The continuity equation obtained from the conservation of mass is given by

$$\frac{\partial \rho}{\partial t} = \rho div(v) = \rho c \tag{4.22}$$

Where ρc is the mass that will be added because of growth and $div(\cdot)$ is the divergence operator.

The density in the current configuration ρ will be defined as

$$J\rho = \rho_0 + \int r_0 \, dt \tag{4.23}$$

Where ρ_0 is the density in the reference configuration and r_0 will be the time rate of change of the density. For this study, the time scale was assumed larger than that of the mechanical loading; therefore growth was calculated one time per day. The density at the current configuration at a time $t_0 \leq t \leq t_1$ will be

$$\rho_1 = \rho_O + r_0 \Delta t \tag{4.24}$$

$$J_1 \rho_1 = \rho_O \tag{4.25}$$

Where ρ_0 and ρ_1 are the densities in the reference and current configuration respectively.

4.2 Biphasic theory

Biphasic theories can be found in [22- 26] that are adapted to Articular Cartilage behavior and will be summarized here. As mentioned before, this theory consists of a tissue formed by a solid phase and a fluid phase (as articular cartilage is). In the following explanation the solid phase will be denote with the superscript *s* and the fluid phase with the superscript *f*. The saturation condition will be met by the volume fractions of each phase.

$$\emptyset^s + \emptyset^f = 1 \tag{4.26}$$

Where $\emptyset^s$ is the volume fraction of the solid phase (GAG, COL) and $\emptyset^f$ is the volume fraction of the fluid phase. The volume fraction of the different constituents, generally denoted by *m*, is

$$\emptyset^m = \frac{\rho^m}{\rho_T^m} \tag{4.27}$$

Where ρ^m will be the apparent density and ρ_T^m will be the true density. As we know density is mass over volume. For the apparent density it will be defined by

$$\rho^m = \frac{mass^m}{tissue\ volume} \tag{4.28}$$

And the true density will be defined as

$$\rho_T^m = \frac{mass^m}{volume^m} \tag{4.29}$$

With equation ($\emptyset^s + \emptyset^f = 1$) and an incompressibility assumption, the continuity equation will now be

$$div(\emptyset^s \mathrm{v}^s + \emptyset^f \mathrm{v}^f) = 0 \tag{4.30}$$

Here v will be the absolute velocity vector of the constituents.

The difference between the constituent's velocities will represent the permeation velocity which will be the relative interstitial fluid found in AC

$$v^{f/s} = v^f - v^s \tag{4.31}$$

The total Cauchy stress of the tissue (both phases) is defined to be

$$\sigma = \sigma^f + \sigma^s \tag{4.32}$$

The constituent stresses are defined per tissue area. This Cauchy stress is also equivalent to the effective stress that ABAQUS uses and is

$$\bar{\sigma}^* = \bar{\sigma} - \chi u_w \mathrm{I} \tag{4.33}$$

Where $\bar{\sigma}$ will be the effective stress of the porous material (solid matrix σ^s), χ will be the saturation which will have a variation between $1 \leq \chi \leq 0$ for when the material is fully saturated or unsaturated, u_w will be the pore pressure of the fluid matrix (σ^f) and **I** is the well-known identity tensor. The biphasic theory used in this study accounts for a fully saturated tissue, therefore χ = 1.

The porosity (*n*) will be the parameter to measure the void spaces in a material, therefore the void ratio is needed, which defined as the ratio of the volume fraction of the fluid phase to the volume fraction of the solid phase.

$$n = \frac{e}{1+e} \tag{4.34}$$

The permeability (*k*) of a material is known as the resistance to the fluid flow through a solid matrix. Such permeability relation was derived in [26] for 1-D strains and is defined by

$$k = k_0 \left[\frac{\emptyset_0^s \emptyset^f}{(1-\emptyset_0^s)\emptyset^s}\right] exp\left[M\left(\frac{\lambda^2-1}{2}\right)\right] \tag{4.35}$$

Where k_0 will be the material permeability and $\emptyset_0^s$ is the initial volume fraction of the solid phase, both in the zero strain configuration. *M* is a non-dimensional permeability constant that describes the exponential increase in permeability with strain, *k* is a positive constant parameter that signifies the rate at which the permeability reaches zero as the solid phase volume fraction reaches 1 and λ is the stretch of the material.

Using equation (4.10) the solid phase volume fraction can be expressed as

$$J\emptyset^s = \emptyset_0^s \rightarrow \emptyset^s = \frac{\emptyset_0^s}{J} \tag{4.36}$$

If the definition of void ratio is entered we will get

$$J = \frac{1+e}{1+e_0} \tag{4.37}$$

Using equation (3.22) permeability can be modified to

$$k = k_0 \left[\frac{e}{e_0}\right]^2 exp\left[\frac{M}{2}\left(\frac{1+e}{1+e_0}\right)^2 - 1\right] \tag{4.38}$$

4.3 Constitutive stresses

The constitutive stresses that are going to be reported are of the 3 main solid matrix components or constituent, glycosaminoglycan (GAG) will account for the pressures formed by

internal swelling due to the negative fixed charged density, collagen (COL) will account for the mechanical responses of the fiber network and the ground substance matrix (MAT) will take into account the different solid matrices components that are not GAG and COL. ABAQUS requires all stresses to be reported as Cauchy stresses and provide the exact material Jacobian matrices (elasticity tensor), these Jacobians are to aid convergence in ABAQUS (guide the computational solver during its iterations). The exact Jacobian matrices were previously developed in [27, 36]. The general equation for the Jacobian matrix in indical notation is

$$\mathbb{C}_{ijkl}^{JAC} = \frac{1}{J}\begin{Bmatrix}\left[\left(\delta_{ik}\delta_{pl} + \delta_{pk}\delta_{il}\right)\sigma_{pj} + \frac{J}{2}\left(\delta_{jk}\delta_{nl} + \delta_{nk}\delta_{jl}\right)\sigma_{in}\right] + \\ \left[\mathbb{C}_{ABCD}F_{iA}F_{jB}F_{kC}F_{lD}\right]\end{Bmatrix} \tag{4.39}$$

δ is the kroenecker delta and σ is the solid matrix Cauchy stress and $\mathbb{C}$ is the material elasticity tensor, which is defined as

$$\mathbb{C} = \frac{\partial \mathbf{S}}{\partial \mathbf{E}} \tag{4.40}$$

S is the second Piola-Kirchhoff stress and **E** is the Lagrangian strain tensor.

The sum of the different constituents of the solid matrix will equal the total solid matrix Cauchy stress

$$\sigma^{SM} = \sigma^{GAG} + \sigma^{COL} + \sigma^{MAT} \tag{4.41}$$

To relate the second Piola-Kirchhoff stress to Cauchy stress we use the following relationship

$$\sigma^{m} = \frac{1}{J}(\mathbf{FSF^{-1}}) \tag{4.42}$$

Where **F** is the deformation gradient tensor of equation (4.3) *J* obtained from equation (4.6) and **S** is the second Piola-Kirchhoff stress tensor.

As mentioned in section 4.1 the solid matrix constituents will occupy an initial (reference) configuration denoted by κ_0^m which will have an initial deformation $\mathbf{F}_0^m$ to meet the

initial stress free solid matrix condition where *m* will denote the different constituents (GAG, COL, MAT).

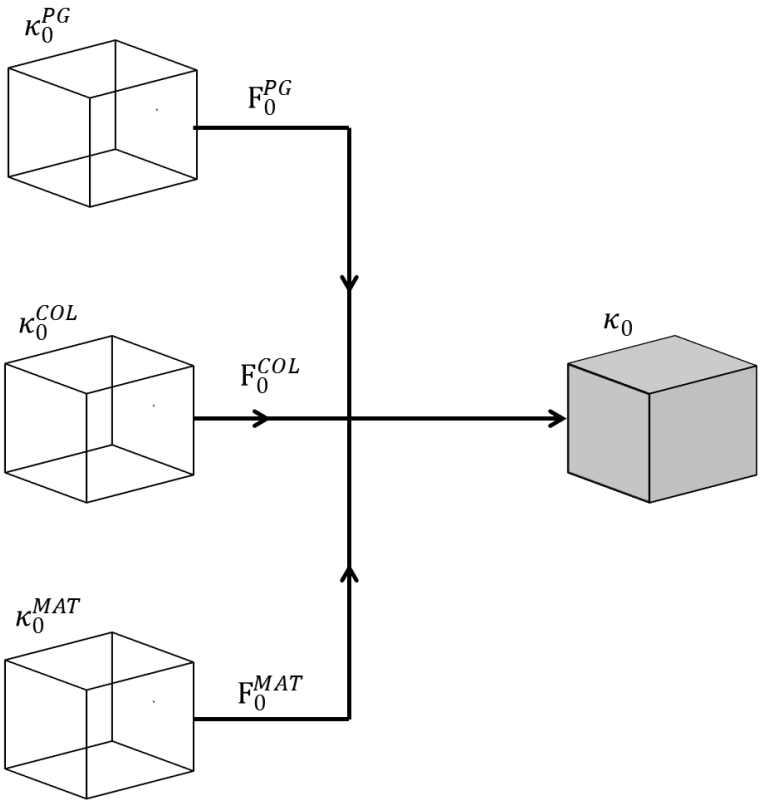

Figure 4.2: The solid matrix must reach a stress free equilibrium condition from the stress free reference configuration of the different constituent elements, for where each will undergo an initial deformation.

4.3.1 Glycosaminoglycan (GAG) stress and Jacobian matrix

The GAG stress is based on a Poisson Boltzmann model developed by Stender et al. [27] fitting it with the experimental data; this resulted in a model of a unit cell and is presented as a Cauchy stress tensor by the following relationship

$$\sigma^{GAG} = -\alpha_1(\rho^{GAG})^{\alpha_2}\mathbf{I} \tag{4.43}$$

ρ^{GAG} is the apparent density of GAG in the current configuration, therefore using the relationship as in equation (4.10) we can relate this apparent density in the current configuration its apparent density in the reference configuration by

$$\rho^{GAG} = \frac{\rho_0^{GAG}}{J} \tag{4.44}$$

For the GAG densities normally seen in immature bovine in articular cartilage it was derived that $\alpha_1 = 2.87$ and $\alpha_2 = 2.5$ [27].

The material elasticity tensor for (GAG), which will be used to establish the Jacobian matrix, was developed in [27] and is

$$\mathbb{C}_{ABCD}^{GAG} = \left(\frac{\alpha\left(\rho_0^{GAG}\right)^{2.5}}{\left(det\left(C^{GAG}\right)\right)^{1.25}}\right)\left(C_{AC}C_{BD} + C_{AD}C_{BC}\right) + 2.5\,\frac{\alpha\left(\rho_0^{GAG}\right)^{2.5} C_{DC}^{-1}C_{AB}^{-1}}{\left(det\left(C^{GAG}\right)\right)^{1.25}} \tag{4.45}$$

This information will be used to implement the different constituent information into the computational model.

4.3.2 Collagen fiber network stress and Jacobian matrix

The collagen material model was developed by Shirazi et al. in [36] and will be briefly summarized below. This model defined the collagen fiber distribution in a unit sphere that will be discretized in pyramidal elements; each pyramid will contain an amount of volume fraction of collagen fibers (pyramids will have different amounts of volume fraction, making this model anisotropic). A continuous distribution of fibers will be defined at every material point.

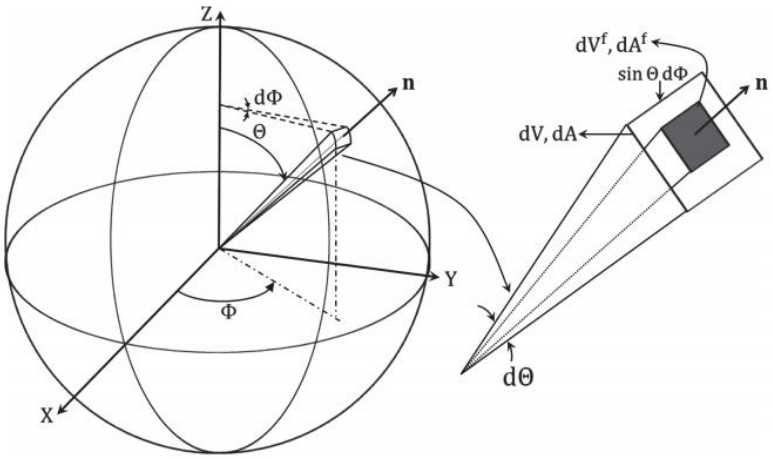

Figure 4.3: Representation of a unit sphere which is used to model collagen fibers in cartilage; this will be defined at each material point to establish a distribution of collagen fibers.

The fibrils that are in a pyramid volume element *dV* will go through a differential area $dA = sin\theta d\theta d\emptyset$, the differential volume *dV* being located at the center of a sphere with *dA* as a surface this differential volume will be

$$dV = \frac{1}{3}dA = \frac{1}{3}sin\theta d\theta d\emptyset \tag{4.46}$$

The total volume fraction of collagen fibrils in the unit sphere is

$$\emptyset_{tot}^{f} = \frac{V^f}{V^{tot}} \tag{4.47}$$

Here, V^f is the volume of the collagen fibers in the unit sphere and V^{tot} is the volume of the unit sphere.

The orientation of the pyramid elements is going to be described by the outward normal vector *n* and because of an assume isotropic distribution of collagen fibers in the unit sphere the volume fraction of collagen fibers in direction n will be

$$\emptyset_{n}^{f} = \frac{dV^f}{dV} = \frac{V^f}{V^{tot}} = \emptyset_{tot}^{f} \tag{4.48}$$

The distribution function of the collagen volume fraction will be defined by

$$R(\theta, \emptyset) = \frac{\emptyset_n^f}{V^{tot}} \tag{4.49}$$

If we integrate the distribution function $R(\theta, \emptyset)$ over the volume we will obtain the volume fraction of collagen fiber

$$\int_V R(\theta, \emptyset) dV = \emptyset_{tot}^f \tag{4.50}$$

With the definitions mentioned above the collagen stress tensor will be described by

$$S^{COL} = \int_{\theta=0}^{\pi} \int_{\emptyset=0}^{\pi} R(\theta, \emptyset)(E_n) H(E_n) \left[\frac{E_f}{2} \left[n \cdot [(C - I) \cdot n] \right] [n \otimes n] \right] \frac{1}{3} sin\theta d\theta d\emptyset \tag{4.51}$$

Where E_n will be the 1-D Lagrangian strain in the outward direction n defined by $E_n = n * \mathrm{E}n$, E_f is the collagen fiber modulus. E is the Lagrangian strain tensor described in equation (4.5). Collagen fibers have been seen to be only mechanically active in tension; because of the tensile load carrying properties of collagen the Heavyside step function denoted by *H* will deactivate such fibers in compression because collagen fibers do not support compression stresses

$$H(E_n) = \begin{cases} 1 & for\ E_n \geq 0 \\ \\ 0 & for\ E_n \leq 0 \end{cases} \tag{4.52}$$

The collagen elasticity tensor used to establish the Jacobian matrix and will be defined by

$$\mathbb{C}^{COL} = \int_{\theta=0}^{\pi} \int_{\emptyset=0}^{\pi} R(\theta, \emptyset) H(E_n) E_f \left[[n \otimes n] \otimes [n \otimes n] \right] \frac{1}{3} sin\theta d\theta d\emptyset \tag{4.53}$$

This information will be used to implement the different constituent information into the computational model.

4.3.2.1 Collagen fiber distribution function. The distribution function derivation was developed in [10, 27, 28] to be able to account for the distribution of the pyramids in the unit

sphere based on collagen content, this distribution, $R(\theta, \emptyset)$, was previously estimated from two dimensional images that were analyzed using qPLM. The unit circle is divided into differential elements with differential area.

$$dA = \frac{1}{2} d\theta \tag{4.54}$$

The area fraction of COL in direction *n* is

$$\gamma_n^f = \frac{dA^f}{dA} \tag{4.55}$$

Here, dA^f is the area of da that is occupied by fibers, and so the total fiber area A^f of the unit circle is

$$A^f = \int_A \gamma_n^f dA \tag{4.56}$$

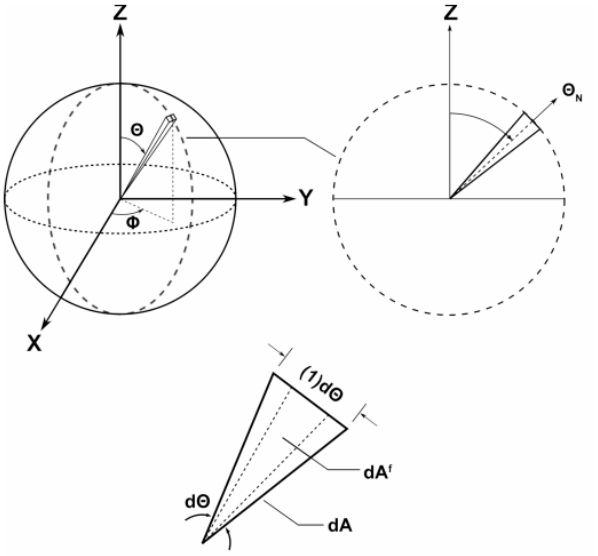

Figure 4.4: Observing the unit sphere in 2-D we have the unit circle, because we are accounting for angle theta only due to symmetry.

The area fraction in direction ***n*** will be dA_n^f normalized by A^f and combining two equations we will have

$$\frac{dA_n^f}{A^f} = \frac{\gamma_n^f dA}{\int_A \gamma_n^f dA} \tag{4.57}$$

This will be subject to the constraint of

$$\frac{1}{A^f}\int_A dA_n^f dA = 1 \tag{4.58}$$

Assuming that Delessee principal will be valid for these differential elements the directional fiber area and the volume fractions will be equal

$$\gamma_n^f = \emptyset_n^f \tag{4.59}$$

qPLM was used to obtained an estimate of the area fraction in the 2-D pyramidal elements (triangles) oriented in mean direction θ_n and range $\Delta\theta_n$ with the area being

$$\Delta A_n = \frac{1}{2}\Delta\theta_n \tag{4.60}$$

Where Δ will denote a finite quantity and all finite triangle elements were assumed to be homogeneous. The semi-circle is discretized into *m* elements with a range of $-\frac{\pi}{2} \leq \theta_n \leq \frac{\pi}{2}$

$$\frac{\Delta A_n^f}{A^f} = \frac{\gamma_n^f \Delta A_n}{\sum_m \gamma_n^f \Delta A_n} \tag{4.61}$$

And

$$\sum_m \frac{\Delta A_n^f}{A^f} = 1 \tag{4.62}$$

Using both equations we will have

$$\frac{\Delta A_n^f}{A^f} = \frac{\emptyset_n^f \Delta A_n}{\sum_m \emptyset_n^f \Delta A_n} \tag{4.63}$$

The value for $\frac{\Delta A_n^f}{A^f}$ is estimated from qPLM for each element. When analyzed through qPLM every pixel is assigned an average angle based on the signal, such pixels are grouped together in different regions of interest (ROI).

The distribution was modeled as Gaussian distribution F_G superposed with a background isotropic distribution F_{nG}, this will ensure that all the elements will have a minimum area fraction to aid convergence. The area fraction distribution will then be

$$\frac{\Delta A_n^f}{A^f} = CF_G(\theta_n) + F_{nG}(\theta_n) \tag{4.64}$$

C is the scalar that will enforce the constraint in equation (4.42). The Gaussian distribution function is defined as

$$f(x) = \frac{e^{-(x-\mu)^2/2\sigma^2}}{\sqrt{2\pi\sigma^2}} \tag{4.65}$$

μ will be the mean of *x* and σ^2 is the standard deviation of *x*, to be able to satisfy the constraint this *f(x)* must be divided by integral $\int f(x)dx$ *f(x) = 1*. This will give us a normalized distribution function

$$f'(x) = \frac{e^{-(x-\mu)^2/2\sigma^2}}{\int e^{-(x-\mu)^2/2\sigma^2} dx} \tag{4.66}$$

Equation (4.50) was adapted for use with unit circle from [59] where

$$\begin{aligned} f'(x) &= F_G(\theta_n) \\ x &= \theta_n \\ \mu &= \alpha_{mean} \\ dx &= \frac{1}{2} d\theta \end{aligned} \tag{4.67}$$

Applying relationships in equation (4.51) to equation of *f'(x)* and integrating from 0 through π we will have

$$F_G(\theta_n) = \frac{e^{-(\theta_n-\mu)^2/2\sigma^2}}{\int_0^{\pi} e^{-(\beta-\mu)^2/2\sigma^2} d\beta} + F_{nG}(\theta_n) \tag{4.68}$$

Where

$$F_{nG}(\theta_n) = \begin{cases} \lambda - F_G(\theta_n) & for\ F_G(\theta_n) < \lambda \\ 0 & for\ F_G(\theta_n) \geq \lambda \end{cases} \tag{4.69}$$

λ is the value of area fraction for the isotropic distribution. Substituting equation (4.52) in equation (4.48) we will have the area fraction distribution function

$$\frac{\Delta A_n^f}{A^f}(\theta_n) = C\left(\frac{e^{-\frac{(\theta_n-\mu)^2}{2\sigma^2}}}{\int_0^\pi e^{-\frac{(\beta-\mu)^2}{2\sigma^2}}d\beta}\right) + F_{nG}(\theta_n) \tag{4.70}$$

The scalar *C* must be solved numerically because the distributions are coupled. Now, the distribution calculated in equation can be used with equation and this will create a system of *m* equations and *m+1* unknowns m values of and this can be solved by applying the constraint in equation (4.42) with an experimental measure of $\emptyset^f$, and so the distribution function of collagen fibers can be defined from $\emptyset_n^f$ obtained by using equation (4.49).

4.3.3 Ground substance matrix (MAT) stress and Jacobian matrix

As mentioned in the early chapters this Ground Substance Matrix (MAT) references the part of the solid matrix that is not GAG or collagen. To model this substance matrix a hyperelastic neo-Hookean solid is used [10, 27], which represents an ideally elastic material and provides ways to model stress strain behaviors that are nonlinearly elastic and defined a material model that is used to predict the same nonlinear stress strain behavior of materials that have large deformations. The stress tensor in second Piola-Kirchhoff notation is

$$S^{MAT} = \mu(\mathbf{I} - \mathbf{C^{-1}}) \tag{4.71}$$

Here, $\mathbf{C^{-1}}$ is the inverse of the right Cauchy green deformation tensor given in equation (4.4), and μ is the shear modulus of MAT. This tress tensor has to be transformed to Cauchy stress using the relationship in equation (4.27).

The elasticity tensor used to establish the Jacobian matrix was derived in [46] and is described by

$$C_{ABCD}^{MAT} = \mu[C_{AC}^{-1}C_{BD}^{-1} + C_{AD}^{-1}C_{BC}^{-1}] \tag{4.72}$$

Or as direct notation

$$C^{MAT} = \mu[C^{-1} \otimes C^{-1} + C^{-1} \otimes C^{-1}] \tag{4.73}$$

This information will be used to implement the different constituent information into the computational model.

4.3.4 Immobility constraint

Since it is assumed that, in the solid matrix, all the constituents (GAG, COL, and MAT) are bound to it and not allowed to move in the tissue, the constituents will present the same deformation, therefore we will have the following relationship

$$F^{SM} = F^{GAG} + F^{COL} + F^{MAT} \tag{4.74}$$

Where we know that SM is Solid Matrix, therefore F^{SM} is the solid matrix deformation tensor that is relative to the stress free configuration and similarly F^{GAG}, F^{COL} and F^{MAT} are the constituents deformation gradient tensor.

4.4 Collagen remodeling – post hoc approach

As we mentioned in section 2.1 a Post Hoc approach is the identification of patterns or relations between experimental measurements and predicted computational outputs; in our study we are to determine patterns or relation between predicted mechanical parameters such as maximum fiber strain, fluid velocity, stress, and experimentally measured collagen fiber distribution. Buschmann et al. in [29] performed studies to determine that GAG (aggrecan) synthesis (i.e. GAG remodeling) is correlated by relative interstitial fluid velocity; similar theoretical approach were applied as dynamic unconfined compression was performed in articular cartilage tissue as well. They studied experimentally-measured results and predicted mechanical parameters obtained computationally and observed patterns between experimental

results of GAG (aggrecan) synthesis and computational predictions of fluid velocity. Regions that showed an experimental increased GAG (aggrecan) synthesis also experienced an increase in interstitial fluid velocity [29]. This same procedure is what our study will be focused on; having our constitutive stresses explained through different sections of this chapter they will be implemented in our computational models from where we will obtain predicted mechanical parameters and derive patterns between experimental measurements of collagen and different predicted mechanical parameters to be able to suggest the trigger of collagen fiber network remodeling.

4.5 Computational implementation

UMAT stands for user material; this is a user material subroutine that is used in ABAQUS when materials have complex behaviors that are not (and cannot be) natively defined in ABAQUS. Articular cartilage is one of those complex materials, since the tissue is nonlinear inhomogeneous, anisotropic and has multiple constituents such as GAG, COL and MAT, which have been previously defined throughout this work. UMAT will let the user define the different tensors, equations and relationships to account for all of these constituents. Our study is based on previous user material subroutines developed in [10], [27] and [28]. These previous works accounted for an isotropic collagen fiber distribution, but, as in [10], this model will account for an anisotropic collagen fiber distribution. Additionally, studies performed in [10] used a user defined field subroutine (USDFLD) to establish and apply remodeling laws to store and update state variables for collagen volume fraction distribution function and GAG density. This UMAT has been updated and will not take into account the USDFLD subroutine to define remodeling laws, but rather to obtain fluid velocity, porosity and relative fluid velocity and store calculated

fiber strain of the different pyramids of the unit sphere to study as predicted outputs. Also, GAG density is no longer a state variable (a parameter that needs to be updated through UMAT) but rather given as a material property (PROPS); the collagen volume fraction distributions, $R(\theta, \emptyset)$, are still assigned a state variable number but will only serve as input to the model for each day as they will not be updated within the USDFLD subroutine.

ABAQUS (v6.12-3) is the finite element analysis (FEA) software that is used to which the material properties assigned to UMAT will pass onto ABAQUS to calculate the different stresses, strains, and other mechanical parameters at each increment to obtain predicted outputs.

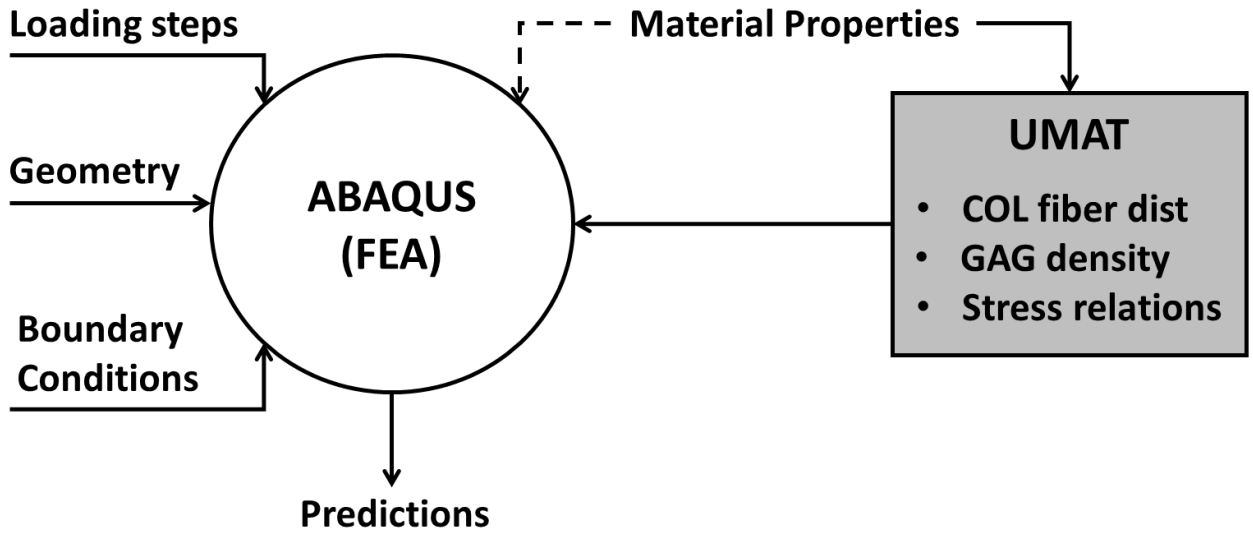

Figure 4.5: Geometry, boundary conditions loading steps and material properties must be given to ABAQUS to be able to obtain prediction of results. UMAT is used to assign complex material properties.

4.6 Geometry, mesh creation and boundary conditions

We have to provide a geometry shape to ABAQUS to be able to create a mesh an thus perform an analysis; experimentally we have a cartilage disk, when the disk is experimenting tissue growth we can observe that there is no movement of the tissue in the **X** and **Y** axis (i.e.

along its axis) (circumferential symmetry) (figure 4.6), therefore we can use symmetry to reduce the cartilage disk to a quarter-disk.

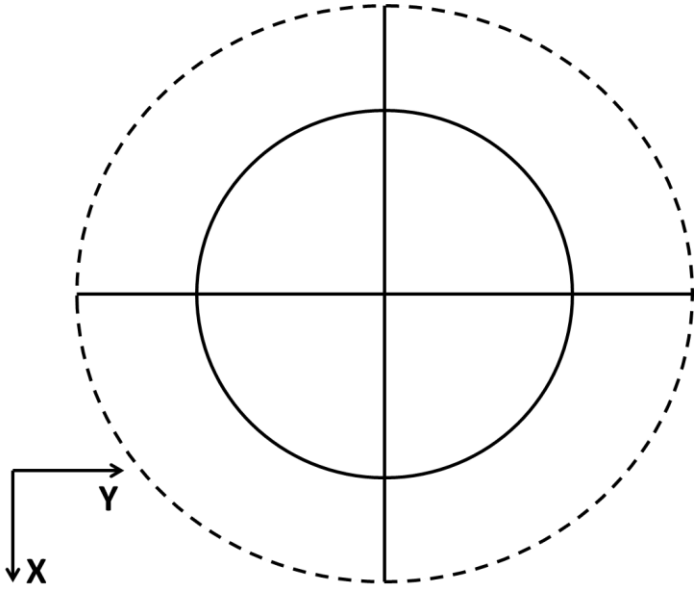

Figure 4.6: Tissue growth representation to justify the use of symmetry to reduce the cartilage disk model to a quarter-disk. Dashed lined represents the deformed cartilage disk.

The mesh that was used in our study was one previously developed in [28] and used in [10] and [29]; it has been validated through different subsequent studies to proportionate the best results with the best computational time. And so a seed of 10 elements was specified along the radius and height of the quarter-disk, this resulted in 960 elements; convergence to this number of elements has been studied previously and has been selected to be the appropriate number for the computational models. The element type used in the analysis is a trilinear coupled stress-pore pressure (C3D8P), also validated through previous studies.

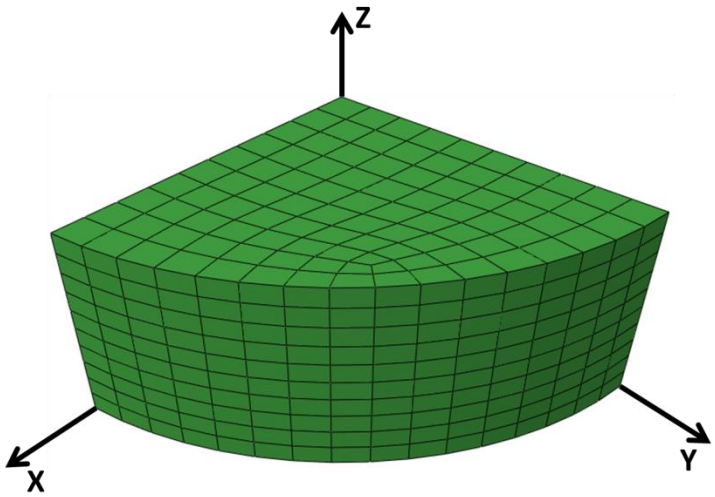

Figure 4.7: Computational representation of a quarter-disk with the 960 assigned elements.

The constraints are applied in the lateral and bottom faces denoted by (-1,0,0), (0,-1,0) and (0,0,-1) in the outward normal direction (i.e. the cartilage cannot move in the **Y** axis normal to the left face, it cannot move in the **X** axis normal to the right face and cannot move in the **Z** axis normal to the bottom face) and a 0 MPa pore pressure is assigned to the curved face of the quarter-disk, having the permeability of the material be dependent on strain; the displacements (strains) mentioned in section 3.1 are applied to the top surface of the quarter-disk.

4.7 Material properties

The user material subroutine UMAT will require different material properties, such as, collagen fiber modulus E_f, initial GAG density ρ_0^{GAG}, shear modulus μ of the Ground Substance Matrix (MAT) and collagen volume fraction distribution, the latter was discussed in *section 4.3.2.1*. The fiber modulus E_f and the initial parameter to determine the initial $R(\theta, \emptyset)$ (i.e. for Day 0) were obtained from [37], μ was obtained from [38] and GAG density ρ_0^{GAG} was obtained from [36].

The parameters for day 6 were obtained from [10]. As we are performing our studies for each day of culture (day 1through day 6) and we only possess data for day 0 and day 6 (because the samples can't be taken out while performing the experimentation), we used a linear interpolation to obtain experimental data for days 2 through 5 (linear interpolation was chosen, because previous studies have done experiments through day 12 and from data obtained for day 0, day 6 and day12 a linear variation of values has been seen) to be able to use as input for our different computational models. Since day 0 is untreated cartilage sample data, the initial data for day 1 is the same data as day 0.

Table 4.1: Experimental data for GAG and collagen density for day 0 and day 6. A linear interpolation was used to determine GAG and collagen density for days 2 through 5.

Day of culture	GAG DENSITY INTERPOLATION (%ww)	COL DENSITY INTERPOLATION (%ww)
0	3.710	9.410
1	3.710	9.410
2	4.908	10.608
3	6.106	11.806
4	7.304	13.004
5	8.502	14.202
6	9.700	5.060

Table 4.2: Material properties required for the computational models. The angle (α) and standard deviation provided are for day 0.

E_f	μ	α_{mean}	$\alpha_{st.dev.}$	λ
224.4 MPa	0.11 Mpa	90°	14.3	0.002543

Table 4.3: Average collagen fiber angles for day 6, for the different regions of interest (ROI). This data, alongside the initial fiber angle data from table 4.3, was used to interpolate and obtain the collagen fiber angles for days 2 through 5.

Day 6											
Region of interest (ROI)											
1		2		3		4		5		6	
Average α [deg.]	St. Dev. [deg.]	Average α [deg.]	St. Dev. [deg.]	Average α [deg.]	St. Dev. [deg.]	Average α [deg.]	St. Dev. [deg.]	Average α [deg.]	St. Dev. [deg.]	Average α [deg.]	St. Dev. [deg.]
91.42352	9.019563	92.62433	9.759159	92.68548	11.18438	89.30463	15.59406	89.59476	16.60600	90.59808	15.06753

4.8 Spherical discretization using pyramids

The unit sphere discussed in in *section 4.3.2* is discretized into 1600 pyramidal elements, this number of pyramids was determined by having $\Delta\theta = 4.5$ and $\Delta\emptyset = 4.5$ this will give us the pyramids for the ranges of $0 \leq \theta \leq \pi$ and $0 \leq \emptyset \leq 2\pi$. The initial volume fractions distribution for each pyramid element for each day of culture were obtained using a MATLAB implementation developed by Yamauchi et al. in [10] using procedures in *section 4.3.2.1*; Kevin Yamauchi used this implementation to obtain the initial distribution $R(\theta, \emptyset)$ of the pyramids (i.e. day 0), we used this implementation to obtain the distribution $R(\theta, \emptyset)$ for each day of culture (i.e. day 1 through day 6) with experimental data provided from our interpolations. Every integration point was assumed to have the same initial collagen fiber volume fraction distribution.

4.9 Simulation steps

This model is simulated to follow the same experimental steps described in section 3.1, i.e. free swelling, ramp (compression) and sinusoidal (dynamic unconfined compression). Each step implements nonlinear geometry due to large deformations.

4.9.1 Free swelling step

Glycosaminoglycan's (GAG) produce a compressive swelling stress that causes the articular cartilage (AC) to be in a nonzero stress reference configuration in the solid matrix, this compressive GAG stress is balanced, by a tensile stress provided by collagen and the ground substance matrix (MAT). The software ABAQUS will solve this balance between the three constituents so that there is a stress free equilibrium in the solid matrix. Since this is a direct elastic solver step, there is no need to include a pore fluid stress response.

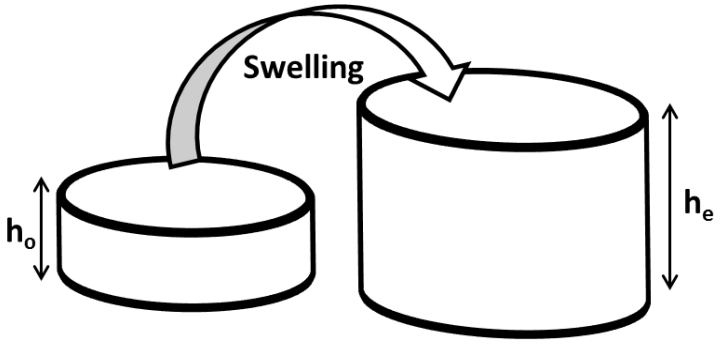

Figure 4.8: ABAQUS will determine the necessary deformation needed for COL and MAT to be able to balance the swelling stress of GAG; this will provide a stress free configuration. The height h_0 is defined experimentally by the samples geometry. The equilibrium height h_e is needed to obtain the displacements/strains used for the subsequent steps.

This step is first needed to calculate the total displacement of the subsequent steps, because they will be affected by h_e (new height).

4.9.2 Ramp step

In this step we applied the 10% compressive strain in unconfined compression to the top surface of the quarter-disk, this is the same continuous loading strain which a static offset that was applied experimentally; the 10% is calculated from the determined new height h_e of the free swelling step. From the experimental procedure the 10% compression was applied at a rate of

$v = 0.001\ mm/s$ and allowed to reach equilibrium for 1200 seconds before the sinusoidal displacement was applied to the quarter-disk. Because it was allowed to reach equilibrium the elastic solver was used, this allows reduction in computational time.

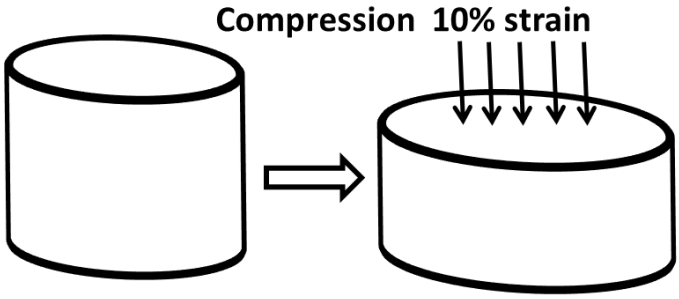

Figure 4.9: A continuous 10% compression is applied to the cartilage disk; the magnitude of the strain is calculated from the new height h_e of the model.

4.9.3 Sinusoidal step

From the experimental setup a sinusoidal displacement is applied to the top surface of the cartilage disk and the same will be applied for this step. The displacement is applied at a frequency of 0.1 Hz and an amplitude of 2% strain in addition to the 10% compression applied in the Ramp step. This is applied for 5 cycles of 10 seconds each, because the quarter-disk reaches steady state by the fifth cycle (i.e. not changing in time after the fifth cycle) as stated in [49]. Since this is the dynamic sinusoidal step a SOILS solver is used to include a pore fluid stress response.

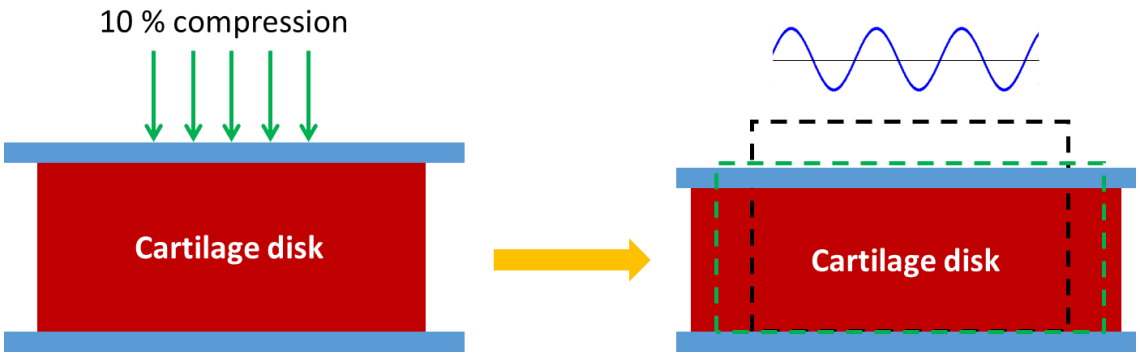

Figure 4.10: A sinusoidal displacement is applied parting from the static offset of the 10% compressive strain applied in the previous step, this magnitude of the displacement is calculated from the new height h_e.

Having mentioned the different steps, one day of culture will account for one free swelling step, one ramp step and one sinusoidal step.

4.10 Solver

A quasi newton solver was used instead of a full newton solver for all steps. Because of the anisotropy of the model and size of the problem while using a full newton solver there were problems with loss of convergence and long computational times.

4.11 Post processing

The retrieval of data and post processing was performed through ABAQUS Visualization module to extract the field output variables from the model for a set of elements chosen that obtained information of the inner and outer region of the cartilage disk (Figure 4.11); this was performed for the 6 models obtaining predicted outputs for the 6 days of experimental culture.

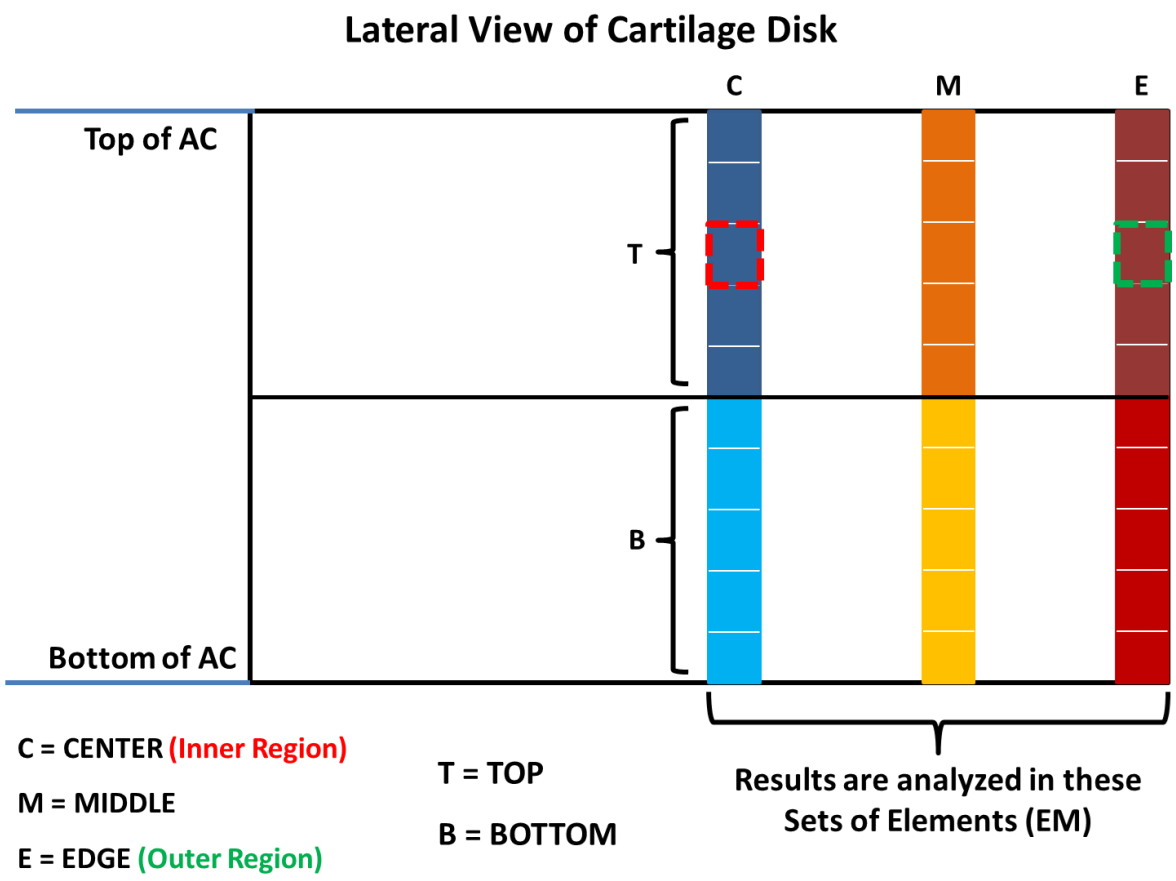

Figure 4.11: The results obtained from the predicted outputs are from the elements located in the Center (inner region) and the Edge (outer region) of the quarter-disk, because of the heterogeneity of the model.

The data extracted was from the 5th 10-second cycle

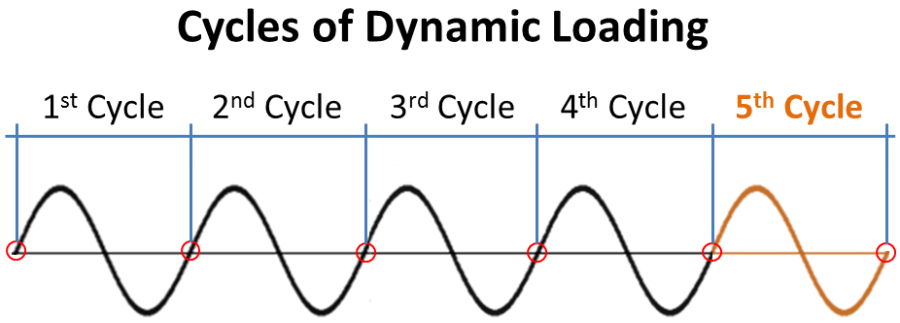

Figure 4.12: The dynamic loading is applied for 5 cycles of 10 seconds each because after this cycle it reaches steady state; the last cycle is used to study the predicted output obtained.

4.12 Computational requirements

The simulation models were run on a computer desktop with a 2.4GHz Intel Xeon processor with 16GB of RAM memory. Each day of simulation had an approximate run time of 48 hours, because the poroelastic solver cannot be used with parallelization, only one CPU core was used. Each model that represented each day of culture provided an output data base that took 11GB of space in the hard drive totaling 66GB of results.

CHAPTER V

RESULTS

5.1 Interpolation of experimental results

Experimental data of collagen distribution for inner and outer region available for day 0 and day 6 were interpolated to estimate the distributions for days 1 to 5 as shown in Figure 5.1 and 5.2. We can then compare change in patterns of predicted mechanical parameters from one day of culture to another with experimentally-observed change in pattern of collagen distribution.

Initially in the first day, collagen fibers were observed to be homogenously distributed throughout cartilage. As shown in Figure 5.1 and Figure 5.2, the volume fraction and distributions are identical for inner and outer regions. At the end of culture, i.e. day 6, the volume fraction of the inner region decreases only 25% while the change in degree of anisotropic distribution of collagen network is not notable. In the outer region, however, the volume fraction decreases 50% from day 1 to day 6 and the degree of anisotropy decreases and moves towards isotropic distribution.

It is worth to note that experimental measurements for day 0 show a high content of collagen fibers are parallel or almost parallel to the articular surface (i.e. $\theta=90°$). At the end of culture, i.e. day 6, the collagen fiber content were observed to be re-oriented away from being parallel to articular surface towards vertical direction (i.e. $\theta=0°$).

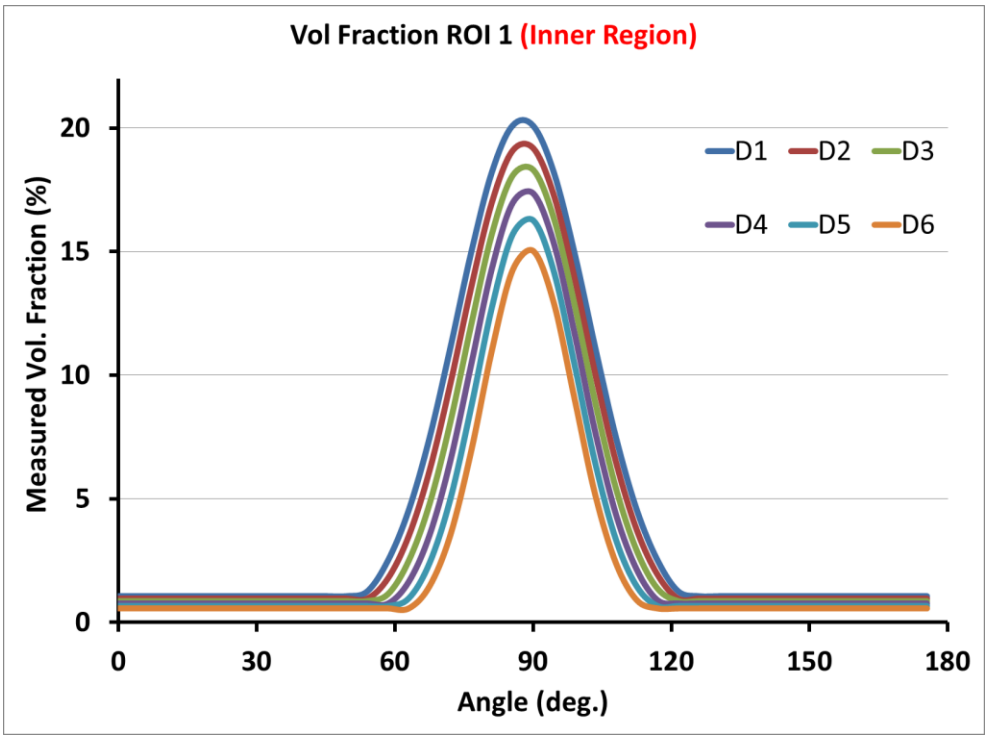

Figure 5.1: Experimental results of collagen volume fraction in the inner region of the cartilage disk. For our studies 90° was established as being parallel to the articular surface.

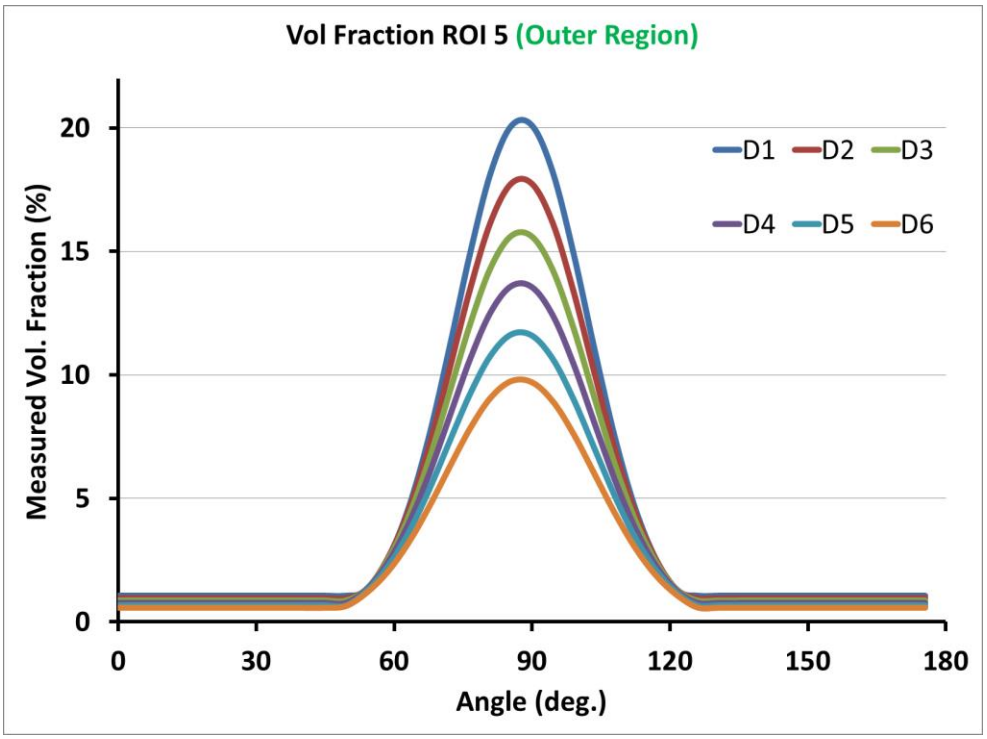

Figure 5.2: Experimental results of collagen volume fraction in the outer region of the cartilage disk. For our studies 90° was established as being parallel to the articular surface.

5.2 Finite element analysis predictions

Predicted outputs of fiber strain, fluid velocity, pore pressure, normal and shear stresses, and logarithmic strains were obtained from our computational studies and studied for the 6 models.

Previous studies suggested that maximum fiber strain could be related to the re-orientation of collagen fibers in articular cartilage (i.e. collagen remodeling) [10, 19, 20]. Kevin Yamauchi [10] validated the remodeling of GAGs in their finite element models by comparing their predictions against experimental data. They were, however, unable to validate the predictions against experiment for collagen remodeling.

The maximum fiber strain for the inner and outer region of the quarter-disk for the 6 computational models (i.e. the 6 days of culture) are depicted in figures 5.3 and 5.4, respectively. Fiber strain increases from day 1 to day 6 as collagen volume fraction decreases. Specifically, in day 1 and for both inner and outer regions (figures 5.3 and 5.4), a higher content of fibers exist parallel to the articular surface providing more resistance and consequently resulting in smaller fiber strain in that direction ($\theta=90°$). Fiber strain may then be inversely related to volume fraction of collage fibers as we compare patterns in figures 5.3 and 5.4 with those in figures 5.1 and 5.2.

Because these models are analyzed as poroelastic models we can study the predicted output results of pore pressure which are presented in figures 5.5 and 5.6. In the first day, we observe a (45%) higher pore pressure in the inner region of the cartilage disk (figure 5.5) than in the outer region (figure 5.6). Pore pressure is higher in the inner region of the cartilage disk as water would need much longer time to move outward and be expelled out of tissue under loading. In the outer region, however, water needs much less time to exit the tissue considering

the boundary condition (zero pore pressure) of the outer curved surface of the disk. From day 1 to day 6, we observe a decrease in pore pressure in both the inner region (10%) and outer regions (75%). There might be a similar pattern between predicted pore pressure shown in figure 5.5 and 5.6 and experimental measurements of collagen volume fraction presented in figure 5.1 and 5.2.

Stresses and strains are important parameters to study in articular cartilage; it is a possibility that either stresses or strains in the cartilage tissue might hold answer in understanding collagen remodeling. In the first day, figures 5.7 and 5.8 shows the predicted stress in the radial direction. Radial stress decreases (18%) as we go from inner to outer region. From day 1 to day 6, the radial stress decreases15% in the inner region and 25% in the outer region. There might be a similar pattern between predicted radial stresses shown in figures 5.7 and 5.8 and experimental measurements of collagen volume fraction presented in figures 5.1 and 5.2. Although changes in the radial stress as we go from day 1 to day 6 for both inner and outer regions are smaller than changes in pore pressure, radial stresses may also contribute to remodeling of collagen fibers.

Shear stresses and shear strains were also predicted from our computational models for the 6 days of culture, however, since we are applying uniform compression to the top surface of the cartilage disk, shear strains and hence shear stresses within the tissue are practically zero.

Previous studies [10, 29] have used computational models to validate fluid velocity to trigger remodeling of Glycosaminoglycan's (GAG) after the velocity passes a certain threshold (60 μm/s). The above studies predicted an increase in fluid velocity from inner region to outer region which corroborates our computational model predictions (figures 5.9 and 5.10). In terms of collagen remodeling, however, fluid velocity has no distinct pattern to be correlated with experimental measurements of collagen volume fraction.

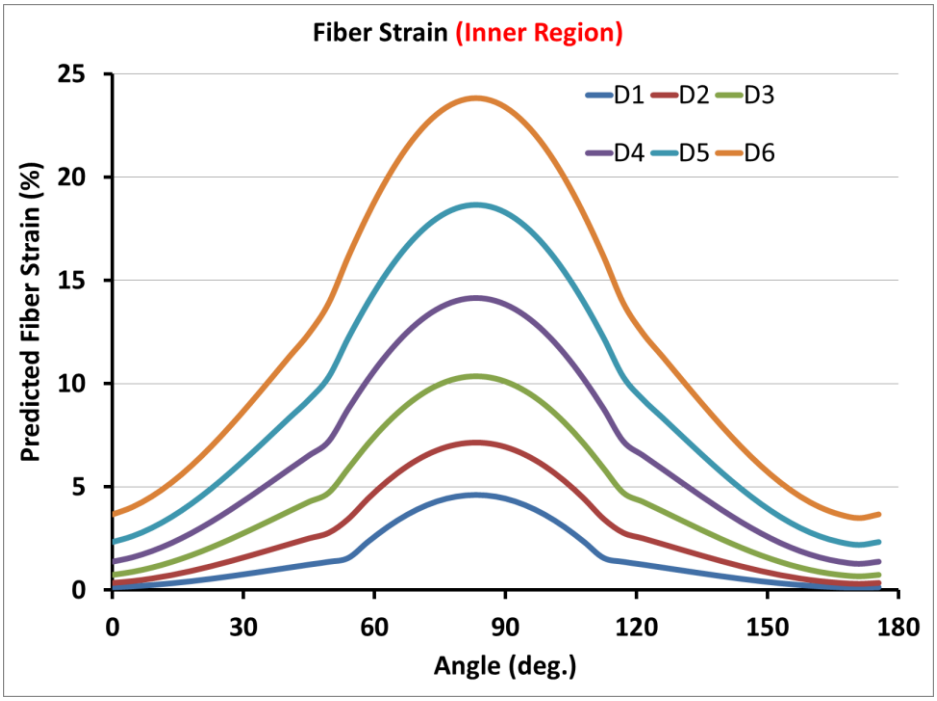

Figure 5.3: Computational prediction of maximum fiber strain in the inner region, obtained for each pyramidal element of the unit sphere. We see an increase in strain throughout the 6 days of culture.

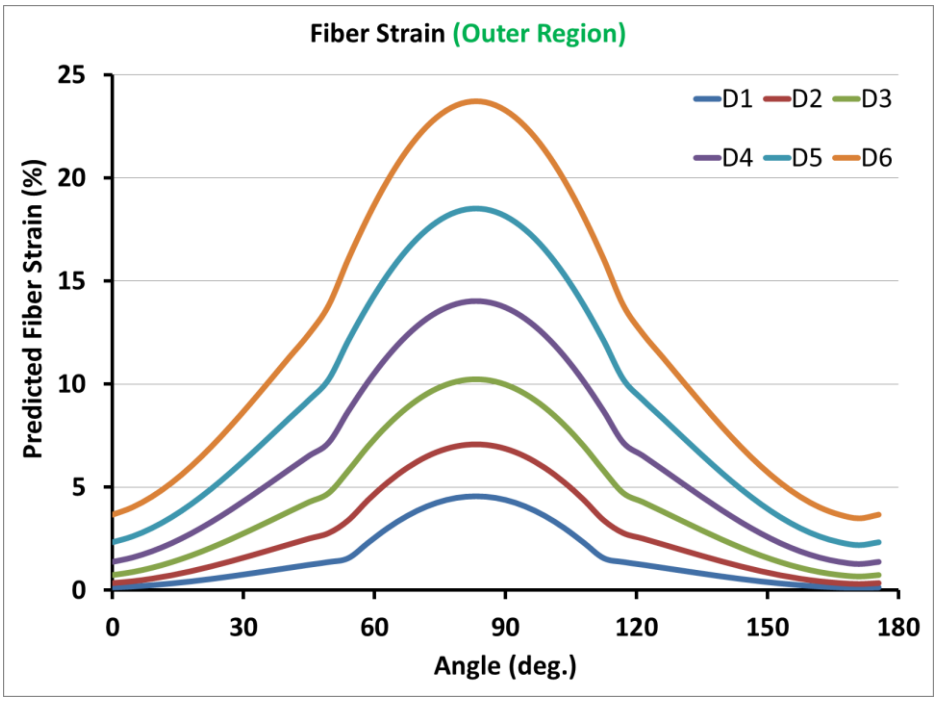

Figure 5.4: Computational prediction of maximum fiber strain in the outer region, obtained for each pyramidal element of the unit sphere. We see an increase in strain throughout the 6 days of culture.

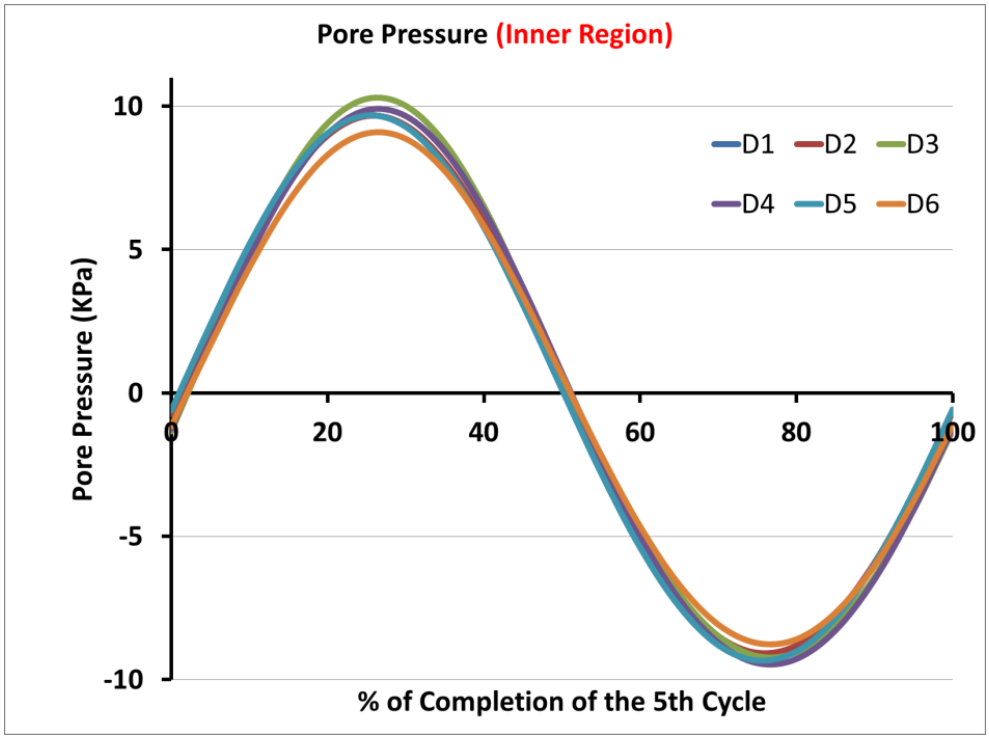

Figure 5.5: Computational prediction of pore pressure in the inner region of the cartilage disk, for the 5th cycle of dynamic loading for 6 days.

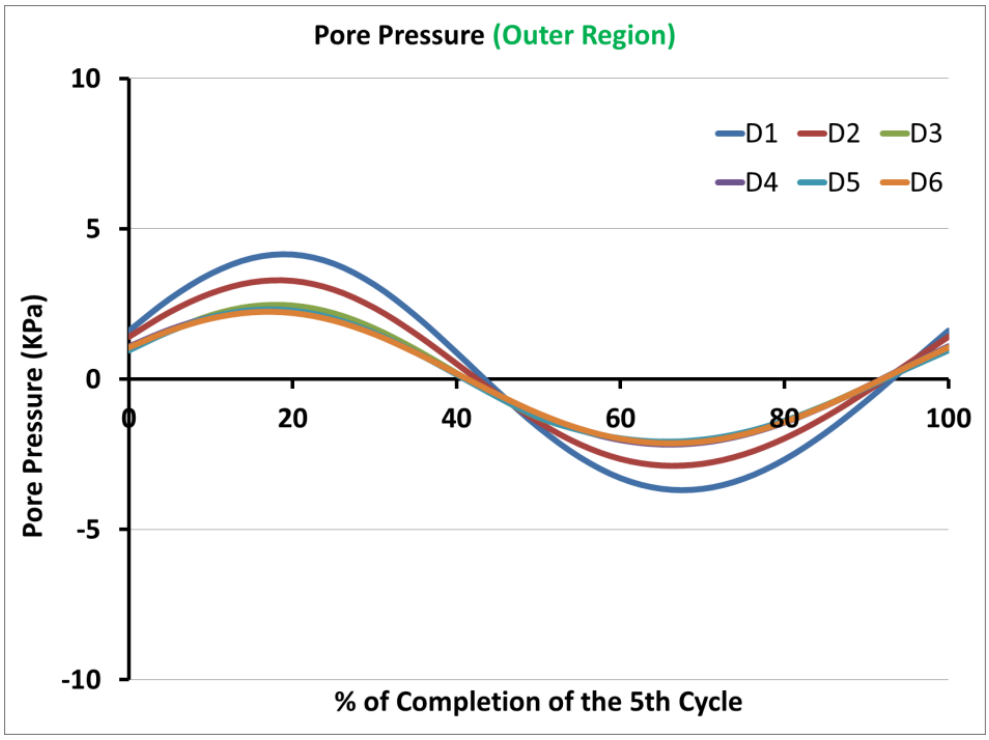

Figure 5.6: Computational prediction of pore pressure in the outer region of the cartilage disk, for the 5th cycle of dynamic loading for 6 days.

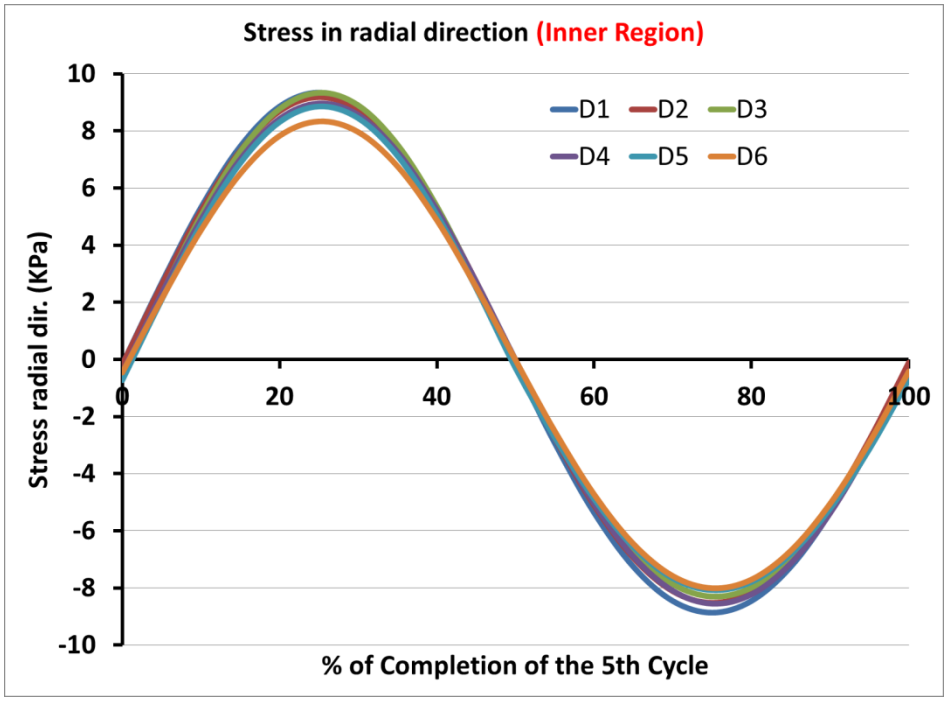

Figure 5.7: Normal stress in the radial direction in the inner region. Results obtained from computational predictions of AC models, for the 5th cycle of the dynamic loading step for each day of culture.

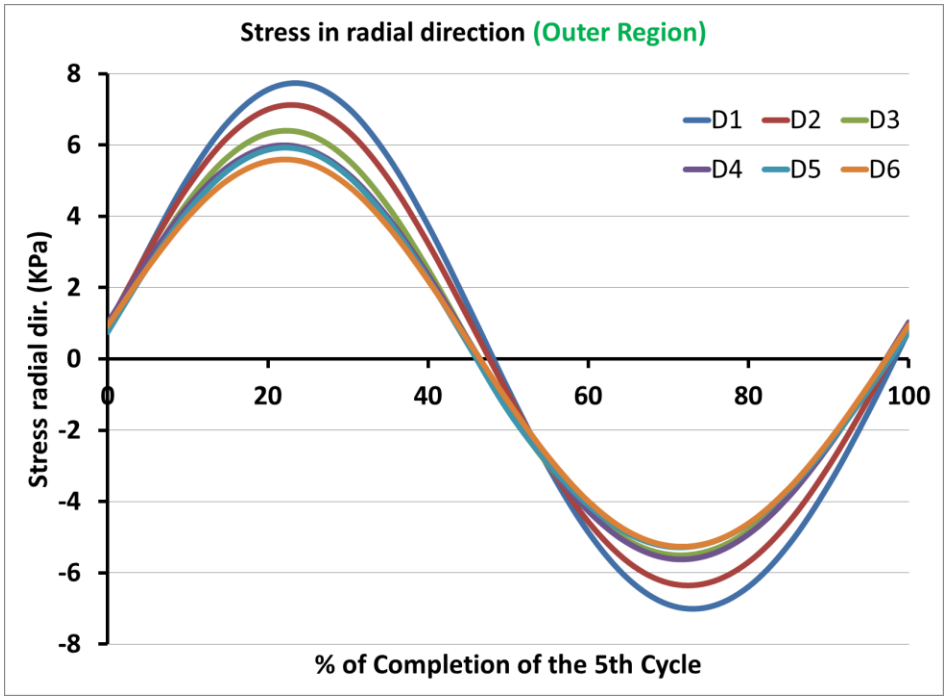

Figure 5.8: Normal stress in the radial direction in the outer region. Results obtained from computational predictions of AC models, for the 5th cycle of the dynamic loading step for each day of culture.

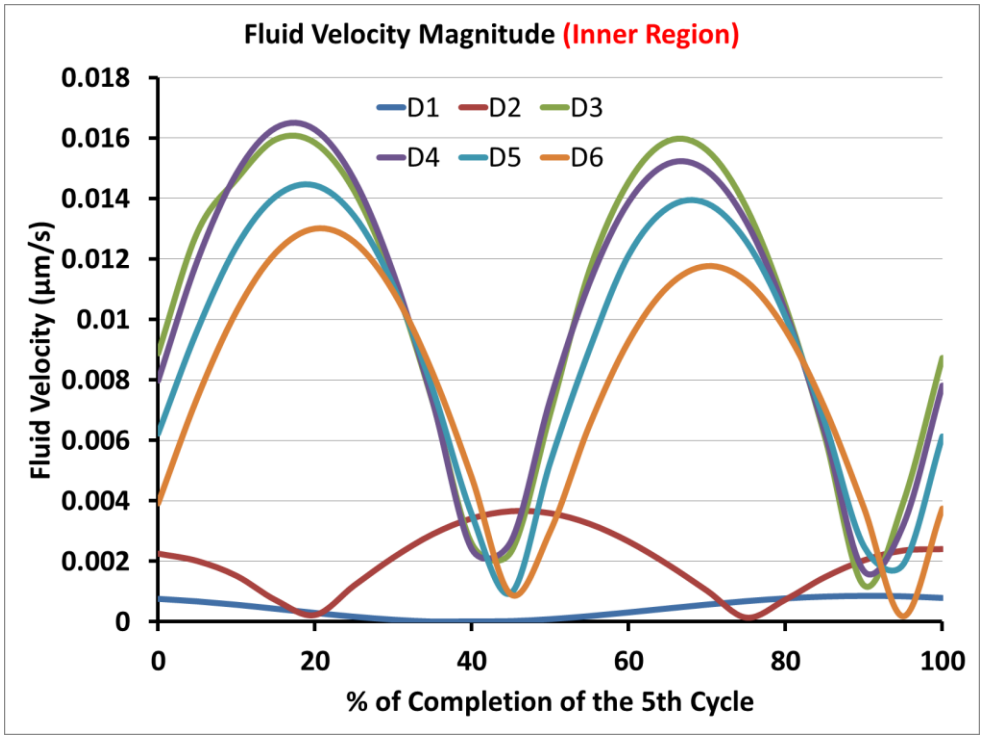

Figure 5.9: Fluid velocity magnitude experienced within the cartilage tissue in the inner region, accounted for the 5th cycle of the dynamic loading step for the 6 days.

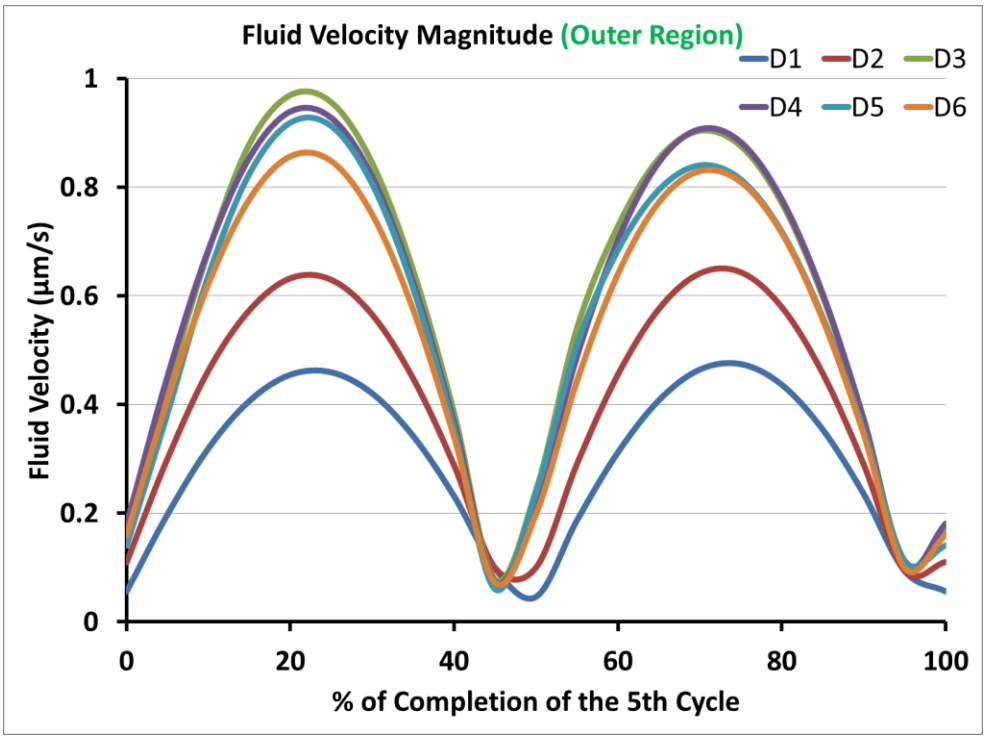

Figure 5.10: Fluid velocity magnitude experienced within the cartilage tissue in the outer region, accounted for the 5th cycle of the dynamic loading step for the 6 days.

5.3 Correlations between experiment and theory

After discussing the predicted mechanical parameters in section 5.2, we can correlate such paramaters with experimental measurements of collage volume fraction (i.e. collagen distribution). These correlations can be seen in figures 5.11 through 5.16. and can provide a better understanding between the paramaters.

Predicted pore pressure and radial stress showed similar trend, i.e. decreasing from day 1 to 6, as in collagen volume fraction for both inner and outer regions (figures 5.11 to 5.14).

Predicted fiber strain, increased from day 1 to 6, was in an inverse relationship with collagen volume fraction for both inner and outer regions (figures 5.15 and 5.16)

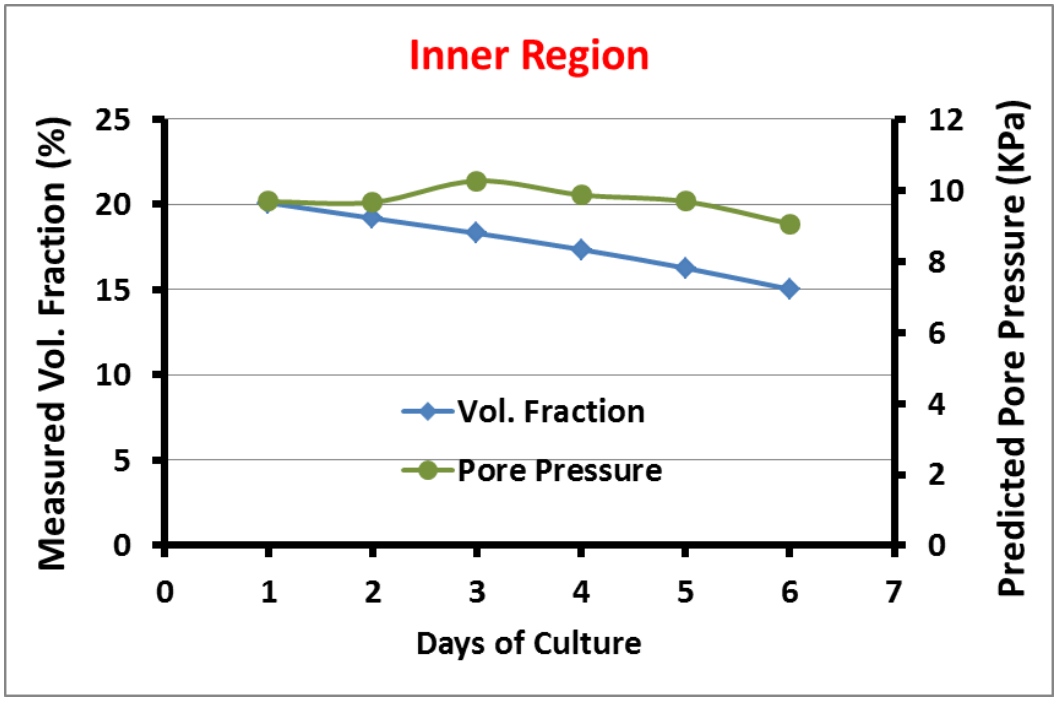

Figure 5.11: Changes in measured volume fraction and predicted pore pressure in the inner region of cartilage during six days of culture.

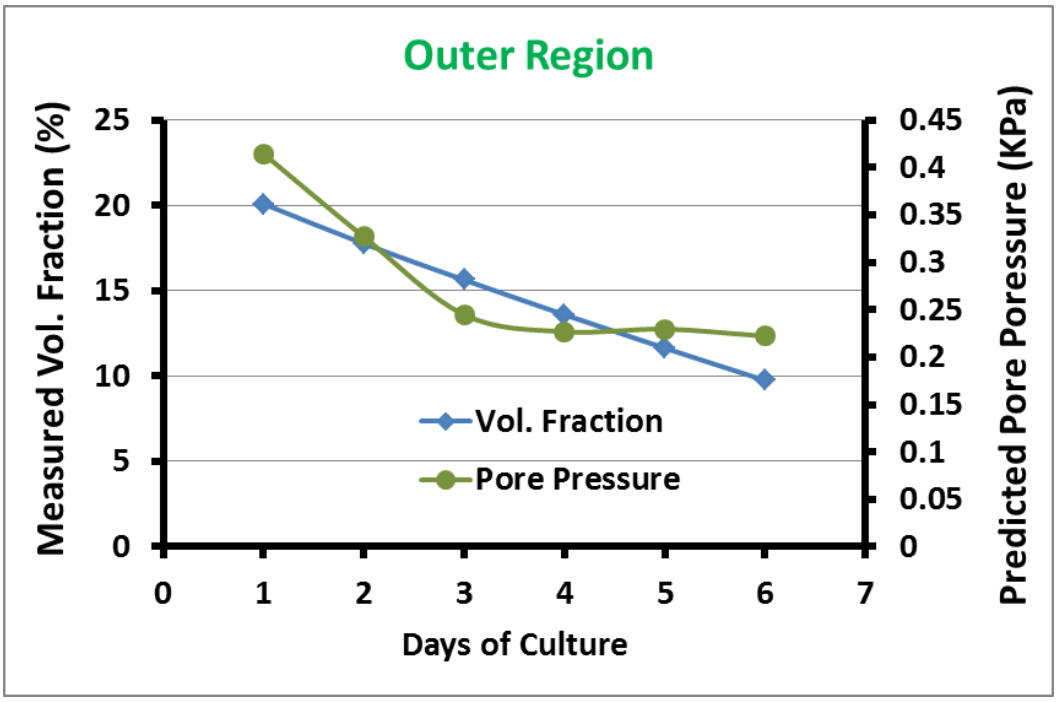

Figure 5.12: Changes in measured volume fraction and predicted pore pressure in the outer region of cartilage during six days of culture.

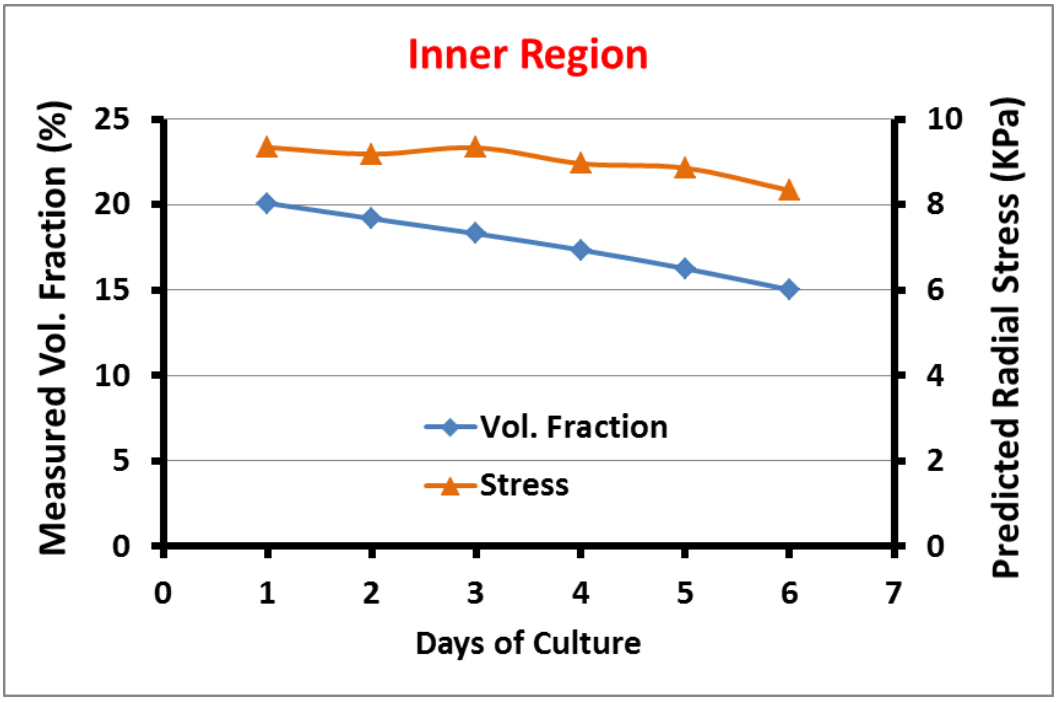

Figure 5.13: Changes in measured volume fraction and predicted radial stress in the inner region of cartilage during six days of culture.

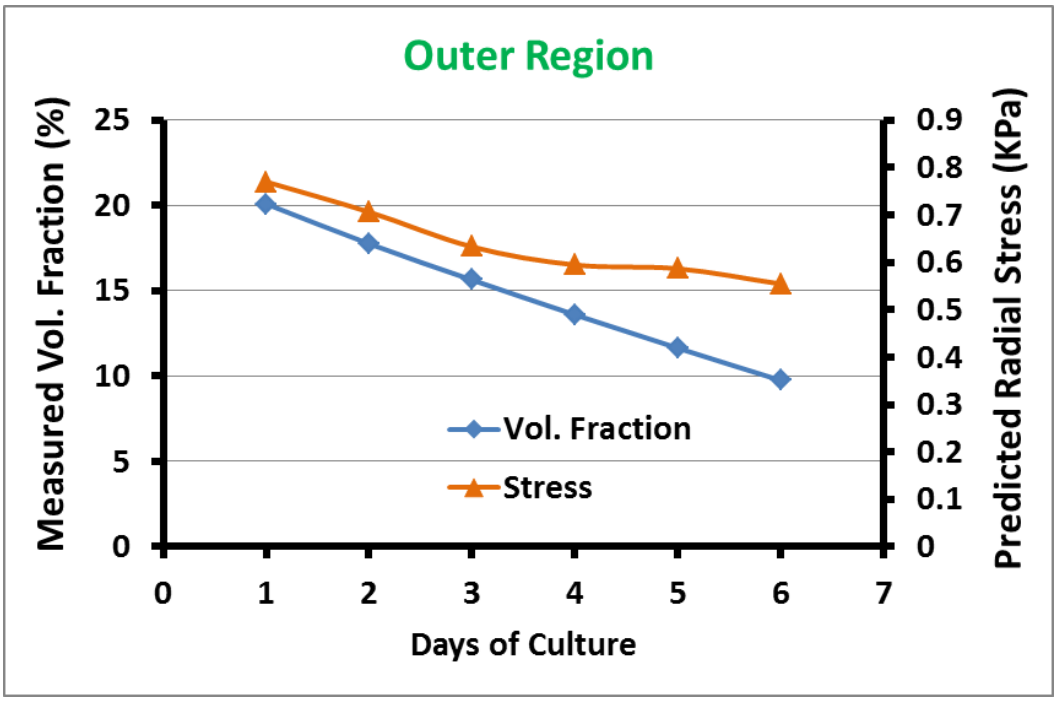

Figure 5.14: Changes in measured volume fraction and predicted radial stress in the outer region of cartilage during six days of culture.

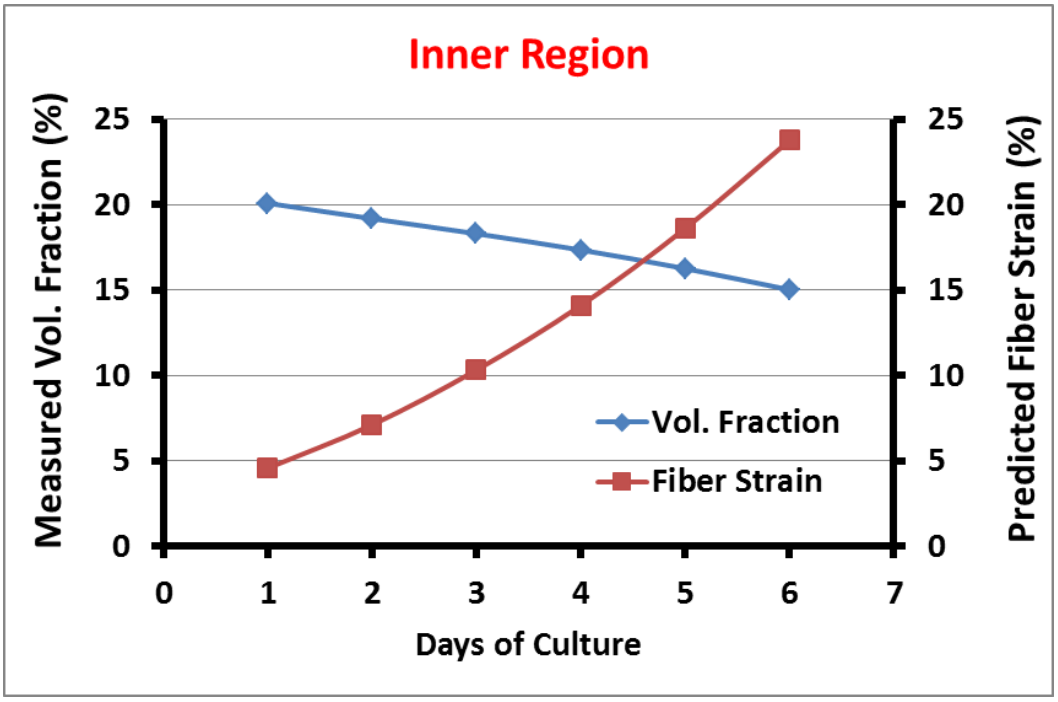

Figure 5.15: Changes in measured volume fraction and predicted fiber strain in the inner region of cartilage during six days of culture.

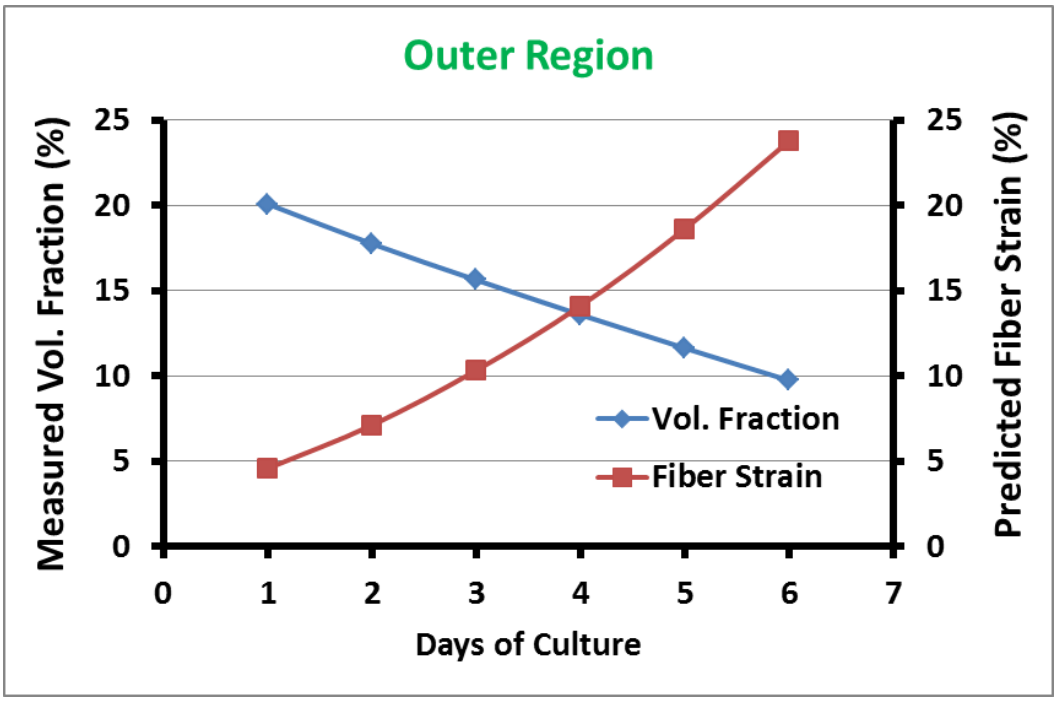

Figure 5.16: Changes in measured volume fraction and predicted fiber strain in the outer region of cartilage during six days of culture.

CHAPTER VI

DISCUSSION

Computational models of articular cartilage were developed to identify patterns between predicted mechanical parameters and experimentally-measured collagen volume fraction (i.e. distribution) for 6 days of culture during dynamic unconfined compression. The experimental measurements of collagen distribution showed that the outer region has a lower degree of anisotropy compared to the inner region at the end of culture. In other words, some of fibers in the outer region gets reoriented and incline towards vertical position after day 6.

Mechanical parameters have been studied as possible triggers [29] for remodeling of AC. Maximum fiber strain, fluid velocity, pore pressure, and radial stress were the identified parameters in the current study to significantly change when collagen structure changes from day 1 to day 6.

A remodeling criteria based on fiber strain was not successful in accurately predicting the change in orientation of collagen fibers in articular cartilage [10], i.e. computational predictions of collagen volume fraction were not in agreement with experimental measurements. Fiber strain in the current study was predicted to increase as the volume fraction of collagen decreases from day 1 to day 6, an inverse relation between the two.

Swelling pressure induced by GAG is resisted by collagen fibers in tension [12,16,17,39]. Previous studies by Aspden et al. [39] suggest that AC functions in a similar way to a pressure vessel, where the internal pressure (GAG) is resisted by tension in the walls (collagen). In

addition, the collagen fibers are oriented in a certain way to be able to tolerate (resist) damage (stress) or internal pressure that the tissue or collagen fibers are experiencing. Stress may be a key to understanding the re-orientation of the fibers within the tissue (i.e. collagen remodeling) in the inner and outer region. In section 5.2, we predicted pore pressure and radial stresses acting in the tissue and derived a correlation with similar pattern between these mechanical parameters and experimentally-measured collagen volume fraction. As collagen volume fraction decreases from inner to outer region, so will the pore pressure and radial stresses. It is possible that pore pressure and/or radial stresses are the mechanical parameters that trigger the reorientation of collagen fibers from inner to outer region (i.e. collagen remodeling).

Kevin Yamauchi [10] indicated that previous studies have been able to model fiber reorientation in collagen gels using growth laws based on the Laplacian of Cauchy stress or strain [19]. It was proposed [10] to investigate a remodeling law based on the Laplacian of fiber stress or strain. This proposed remodeling algorithm relates to what we have concluded, i.e. radial stresses and/or pore pressure follow similar pattern as experimentally-measured collagen volume fraction and could be the mechanical parameters that trigger collagen remodeling. Therefore, remodeling laws that can relate pore pressure and stress, in the tissue or in the fibers, with collagen distribution should be investigated.

With that being said, we have two candidates for possible triggers of collagen remodeling in articular cartilage. First, considering that predicted fiber strain is inversely related to experimentally-measured collagen volume fraction, we speculate that some fibers reorient towards vertical position in the outer region when experiencing large strains. Second, due to a decrease in pore pressure and radial stress from the inner region to the outer region, the collagen

fibers wouldn't need to resist high stresses that are acting upon the tissue and therefore they reorient to a different position (i.e. towards vertical).

These two scenarios (candidates) can be further studied by understanding the role of GAG, orientation of collagen fibers and collagen fiber content in articular cartilage tissue by using computational models. These models will give us more insight in the role of collagen fibers in resisting deformation of the tissue.

Articular cartilage is a viscoelastic tissue (time-dependent behavior). A limitation to this study is that it does not account for a viscoelastic solid matrix. Poroviscoelastic models of AC have been successfully used to study mechanical responses of AC in different loading conditions [40, 41] including dynamic unconfined compression. Anisotropic biphasic models have also been used to predict articular cartilage responses during unconfined compression [42]

The current study employs a poroelastic model to focus on the application of dynamic unconfined compression. A viscoelastic solid matrix, however, should be employed for the solid matrix to study a combination of compression, tension, shear and other types of loadings. A review on different constitutive modeling of AC can be found in [43].

An additional limitation of this study is the assumption of isotropic permeability in cartilage. Studies have shown that GAG network geometry can contribute to an anisotropic permeability under compression. As it is seen that permeability decreased more rapidly in a direction perpendicular to the applied compression and decreased more slowly parallel to the direction of compression [44]. Further studies should investigate these changes in permeability and the ability to computationally implement them in future studies when applying compression to the cartilage tissue.

REFERENCES

[1] M. B. Goldring, S. R. Goldring. “Articular cartilage and subchondral bone in the pathogenesis of osteoarthritis”. Annals of the Newy York Academy of Sciences. Skeletal Biology and Medicine. 2010.

[2] J. A. Buckwalter, H. J. Mankin, A. J. Grodzinsky. “Articular Cartilage and Osteoarthritis”. AAOS instructional Course Lecture. Volume 54. 2005.

[3] X.L. Lu, V.C. Mow. “Biomechanics of Articular Cartilage and Determination of Material Properties”. American College of Sports and Medicine. 2008.

[4] J. M. Hootman, C. G. Helmick. “Projections of US prevalence of Arthritis and Associated Activity Limitations”. American College of Rheumatology. Arthritis and Rheumatism. Vol. 54, No 1, pp 226-229. January 2006.

[5] “Morbidity and Mortality Weekly Report” U.S. Department of Health and Human Services. Centers of Disease Control and Prevention. Vol. 58, No. 16. May 2009.

[6] “Morbidity and Mortality Weekly Report” U.S. Department of Health and Human Services. Centers of Disease Control and Prevention. Vol. 62, No. 44. November 2013.

[7] G.M. Williams, S.M. Klisch, R.L. Sah. “Bioengineering cartilage growth, maturation, and form” International Pediatric Research Foundation. Vol. 63 No. 5, 2008.

[8] G. Portocarrero, G. Collins, T. Livinsgton Arinzeh, “Challenges in Cartilage Tissue Engineering”. Tissue Science and Engineering. Volume 4. Issue 1. 2013.

[9] W. Wilson, C. C. van Donkelaar, R. van Rietbergen, R. Huiskes. “The role of computational models in the search for the mechanical behavior and damage mechanisms of articular cartilage”. Medical Engineering & Physics. March 2005.

[10] K. Yamauchi. “Prediction of Articular Cartilage Remodeling During Dynamic Compreccion with a Finite Element Model” Master’s Thesis. Mechanical Engineering Department, California Polytechnic State University. June 2012.

[11] X. Houard, M. Goldring, F. Berenbaum. “Homeostatic mechanisms in articular cartilage and role of inflammation in osteoarthritis”. Curr. Rheumatol Rep. September 2013.

[12] A. Asanbaeva, K. Masuda, E.J. – M.A. Thonar, S.M. Klisch, R.L. Sah. “Cartilage growth and remodeling: modulation of balance between proteoglycan and collagen network in vitro with β-aminopropionitrile” International Cartilage Repair Society. Osteoarthritis Research Society International. 2008.

[13] L. A. Fortier, J. U. Barker, E. J. Strauss, T. M. McCarrel, B. J. Cole. “The role of growth factors in cartilage repair”. Symposium: Clinical Relevant Strategies for treating Cartilage and Meniscal Pathology. Clinical Orthopedic Related Research. Volume 469, Number 10. March/October 2011.

[14] T. Ficklin, G. Thomas, J. C. Barthel, A. Asanbaeva, E. J. Thonar, K. Masuda, A. C. Chen, R. L. Sah, A. Davol, S. M. Klisch. “Articular cartilage mechanical and biomechanical property relations before and after in vitro growth” Journal of Biomechanics. June 2007.

[15] L. Kock, C. C. van Donkelaar, K. Ito. “Tissue Engineering of functional articular cartilage: the current status”. Society of Cell Tissue Research. October 2001.

[16] E. Han, S. S. Chen, S. M. Klisch, R. L. Sah. “Contribution of Proteoglycan Osmotic Swelling Pressure to the compressive properties of Articular Cartilage”.

[17] A. Tomic. “Nonlinear Elasticity, fluid flow, and remodeling in biological tissues”. Master’s Thesis, Department of Mechanical and Manufacturing Engineering. University of Calgary. June 2012.

[18] D. Eyre. “Review: Collagen of articular cartilage”. BioMed Central, Arthritis Research, October 2001.

[19] M. Kroon. “A continuum mechanics framework and a constitutive model for remodeling of collagen gels and collageneous tissues”. Journal of Mechanics and Physics of Solids. March 2010.

[20] N. J. B. Driessen, W. Wilson, C. V. C. Bouten, F. P. T. Baaijens. “A computational model for collagen fibre remodeling in arterial wall”. Journal of Theoretical Biology. August 2003.

[21] F. Massooumian, R. Juškaitis, M. A. A. Neil, T. Wilson. “Journal of Microscopy. Vol. 209, Pt. 1. January 2003.

[22] A. F. Mak. “Biphasic Indentation of Articular Cartilage. Theoretical Analysis”. Journal of Biomechanics. Vol. 20, No. 7, pp 703-714. 1987.

[23] P.A. Smyth. “Viscoelastic behavior of articular cartilage in unconfined compression” Master’s Thesis Woodruff School of Mechanical Engineering. Georgia Institute of Technology. May 2013.

[24] P. S. Donzelli, R. L. Spilker, G. A. Ateshian, V. C. Mow. “Contact analysis of biphasic transversely isotropic cartilage layers and correlations with tissue”. Journal of Biomechanics. May 1999.

[25] S. M. Klisch, J. C. Lotz. “A Special Theory of Bihpasic Mixtures and Experimental Results for Human Annulus Fibrious Tested in Confined Compression”. American Society of Mechanical Engineers. Vol. 122, April 2000.

[26] M. H. Holmes, V. C. Mow. “The Nonlinear Characteristics of soft gels and hydrated connective tissue in ultrafiltration”. Journal of Biomechanics. Vol. 23, No. 11, pp 1145-1156. May 1990.

[27] M. E. Stender. “Predicting articular cartilage constituent material properties following in vitro growth using proteoglycan-collagen mixture model”. Master’s Thesis. Mechanical Engineering Department, California Polytechnic State University. March 2011.

[28] K. K. Kam. “Poroelastic Finite Element Analysis of Heterogeneous Articular Cartilage Explant Under Dynamic Compression in ABAQUS”. Master’s Thesis. Mechanical Engineering Department, California Polytechnic State University. June 2010.

[29] M. D. Buschmann, Y.J. Kim, M. Wong, E. Frank, E. B. Hunziker, A. J. Grodzinsky. “Stimulation of Aggrecan Synthesis in Cartilage Explants by Cyclic Loading is localized to

Regions of High Interstitial Fluid Flow". Archives of Biochemestry and Biophysics. Vol. 366, No. 1, pp 1-7. June 1999.

[30] M. Fortin, J. Soulhat, A. Shirazi-Adl, E. B. Hunziker, M. D. Buschmann. "Un confined Compression of Articular Cartilage: Nonlinear Behavior and Comparison with a Fibril-Reinforced Biphasic Model". Journal of Biomechanical Engineering. Vol. 122. April 2000.

[31] R. W. Farndale, D. J. Buttle, A. J. Barret. "Improved quantition and discrimination of sulphated glycosaminoglycans by use of dymethylmethylene blue". Biochemestry & Biphysics Acta 883. 1986.

[32] J. F. Woessner, Jr. "The Determination of Hydroxyproline in Tissue and Protein Samples Containing Small Proportions of this Imino Acid". Biochemestry & Biphysics Acta 93. 1961

[33] P. J. Basser, R. Schneiderman, R. A. Bank, E. Watchel, A. Maroudas. "Mechancal Properties of the Collagen Network in Human Articular Cartilage as Measured by Osmotic Stress Technique". Biochemestry and Biophysics. Vol. 351, No. 2, pp. 207-219, March 1998.

[34] K. A. Yamauchi. "Use of Biochemical data to determine Model Parameters" for Master's Thesis. Mechanical Engineering Department, California Polytechnic State University. June 2012.

[35] J. N. Reddy. "An Introduction to Continuum Mechanics". Texas A&M University. Cambridge University Press. 2008.

[36] R. Shirazi, P. Vena, R. L. Sah, S. M. Klisch. "Modeling the collagen fibril netwiork of biologiucal tissue as a nonlinearly elastic material using a continuos volume fraction distribution function". Journal of Mathematics and Mechanics of Solids. July 2010.

[37] M. E. Stender, C. B. Raub, K. A. Yamauchi, R. Shirazi, P. Vena, R. L. Sah, S. J. Hazelwood, S. M. Klisch. “Integrating Qplm and biomechanical test data with an anisotropic fiber distribution model and predictions of TGF-β1 and IGF-1 regulation of articular cartilage fiber modulus”. Biomechanic Models and Mechanobiology. December 2012.

[38] N. T. Balcom, B. Berg-Johansen, K. J. Dills, J. R. Van Donk, G. M. Williams, A. C. Chen, S. J. Hazelwood, R. L. Sah, S. M. Klisch. “ In vitro Articular Cartilage Growth with Sequential Application of IGF-1 and TGF-β1 Enhances Volumetric Growth and Maintains Compressive Properties”. Journal of Biomechanical Engineering. Vol. 134. March 2012.

[39] R. M. Aspden, D. W. L. Hukins. “Stress in collagen fibrils of articular cartilage calculated from their measured orientations”. Gustav Fischer Verlag, Stuttgart. Matrix Vol. 9, pp 486-488. 1989.

[40] W. Wilson, C. C. Donkelaar, B. van Rietbergen, R. Huiskes. “A fibril-reinforced poroviscoelastic swelling model for articular cartilage”. Journal of Biomechanics. July 2004.

[41] M. R. DiSilvestro, J. K. Francis Suh. “A cross-validation of the biphasic poroviscoelastic model of articular cartilage in unconfined compression, indentation, and confined compression”. Journal of Biomechanics. November 2000.

[42] M. A. Soltz, G. A. Ateshian. “ A conwise linear elasticity mixture model for the analysis of Tension-Compression Nonlinearity in Articular Cartilage”. Journal of Biomechanical Engineering. April 2010.

[43] C. A. Tayloer, K. Miller. “Constitutive Modeling of Cartilaginous Tissues: Review” Journal of Applied Biomechanics. 2006.

[44] T. M. Quinn, P. Dierickx, A. J. Grodzinsky. “Glycosaminoglycan network geometry may contribute to anisotropic hydraulic permeability in cartilage under compression”. Journal of Biomechanics. May 2001.

[45] L. Danišovič, I. Varga, R. Zamborský, D. Böhmer. “The tissue engineering of articular cartilage: cells, scaffolds and stimulating factors” Society of Experimental Biology and Medicine. January 2012.

BIOGRAPHICAL SKETCH

Juan Andres Coello Amado, is a Mechanical Engineer with a Master's Degree from the University of Texas-Pan American which he started in January 2014 and graduated in July 2015. He obtained his Bachelor's degree in Mechanical Engineering from the Universidad del Zulia in his home country in Maracaibo, Venezuela; he started his bachelors in March 2005 and graduated in March 2011. He designed, built and performed a cost analysis of mechanical creepers as his undergraduate thesis for a company which he was interning as called MAKINT, a Komatsu construction equipment dealer. He began his professional career at MAKINT in September 2009, where he started as an intern developing a new Computer Management Maintenance System (CMMS) for the service department. He later continued working there as degreed mechanical engineer administrating a satellite system called Komtrax, among his accomplishments was the implementation of the new CMMS system at MAKINT, which allowed for a more productive department. He continued his professional career at MAKINT until the year 2013 having been promoted to the Service Department Manager and Supervisor. He then moved on to start his graduate studies at the University of Texas-Pan American where he started working as a Research Assistant under the supervision of Dr. Reza Shirazi. His main work was focused on Biomedical Engineering, more specifically, Tissue Engineering, from where he was able to develop computational models and predict specific behavior of Articular Cartilage; this is a step forward to be able to engineer a fully functional cartilage. His permanent mailing address is Urbanizacion Irama, Calle GH Casa 9-67, Maracaibo, Venezuela, 4002.